THE RAINFALL ATLAS OF HAWAIʻI 2011

Final Report

Thomas W. Giambelluca[1], Qi Chen[1], Abby G. Frazier[1], Jonathan P. Price[2]
Yi-Leng Chen[3], Pao-Shin Chu[3], and Jon K. Eischeid[4]

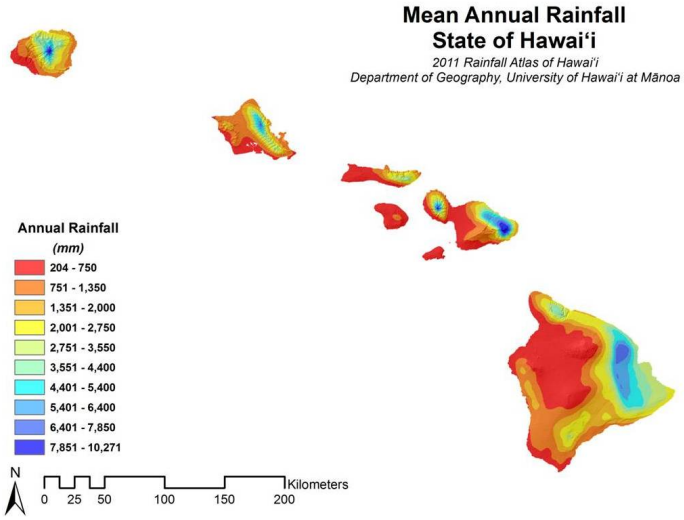

[1]Department of Geography, University of Hawaiʻi at Mānoa, Honolulu, HI, USA
[2]Department of Geography and Environmental Sciences, University of Hawaiʻi - Hilo, Hilo, HI, USA
[3]Department of Meteorology, University of Hawaiʻi at Mānoa, Honolulu, HI, USA
[4]Cooperative Institute for Research in Environmental Science, University of Colorado, Boulder, CO, USA

October 2011

Acknowledgments

The 2011 Rainfall Atlas of Hawai‘i was developed under an agreement between the State of Hawai‘i Commission on Water Resource Management and the U.S. Army Corps of Engineers, Honolulu District under Section 22 of the Water Resources Development Act of 1974. Contract No. W9128A-04-D-0019, Contract Task Order No. 0038 was awarded to Wil Chee Planning, Inc., which subcontracted the work to the University of Hawai‘i at Mānoa, Department of Geography. The development of the 2011 Rainfall Atlas of Hawai‘i was supported by numerous individuals and organizations. Please see the “People” tab of the Rainfall Atlas of Hawai‘i web site (http://rainfall.geography.hawaii.edu) for information about those who contributed to this work. We are grateful to the people listed there, as well as the many other individuals who contributed to Hawai‘i’s rainfall dataset by carefully and consistently making measurements and recording and preserving the data. Those records are an invaluable resource, without which no rainfall map analysis would be possible.

Citing the Rainfall Atlas of Hawai‘i

Please cite this report and any products from the Rainfall Atlas of Hawai‘i website (including screen shots, copied data, saved graphs, downloaded products, and text) as follows:

“Giambelluca TW, Chen Q, Frazier AG, Price JP, Chen Y-L, Chu P-S, Eischeid J., and Delparte, D. 2011. The Rainfall Atlas of Hawai‘i.
http://rainfall.geography.hawaii.edu.”

Introduction

The Hawaiian Islands have one of the most diverse rainfall patterns on earth. The mountainous terrain, persistent trade winds, heating and cooling of the land, and the regular presence of a stable atmospheric layer at an elevation of around 7,000 ft. interact to produce areas of uplift in distinct spatial patterns anchored to the topography. The resulting clouds and rainfall produced by this uplift lead to dramatic differences in mean rainfall over short distances. Knowledge of the mean rainfall patterns is critically important for a variety of resource management issues, including ground water and surface water development and protection, controlling and eradicating invasive species, protecting and restoring native ecosystems, and planning for the effects of global warming.

Why “Rainfall” instead of “Precipitation”?

Precipitation in Hawai‘i includes rain, various types of frozen precipitation, such as snow, sleet, hail, and freezing rain, and fog drip. Frozen precipitation is a minor contributor overall. However, fog drip, derived from direct interception of cloud droplets by vegetation, is a major source of water in the middle-elevation fog zones of Hawai‘i's mountains. We use the term “rainfall” here instead of “precipitation, because, although we include frozen precipitation as a minor component, the other major precipitation component, fog drip, is not included.

The Rainfall Atlas of Hawai‘i is a set of maps of the spatial patterns of rainfall for the major Hawaiian Islands. Maps are available for mean monthly and annual rainfall. The maps represent our best estimates of the mean rainfall for the 30-yr base period 1978–2007. However, for many reasons, it is not possible to determine the exact value of mean rainfall for any location. Therefore, for every map of mean rainfall, we provide a corresponding map of uncertainty. Uncertainty tends to be greatest where we have the poorest information about rainfall, for example in remote locations far from the nearest raingage.

A Rainfall Atlas of Hawai‘i web site (http://rainfall.geography.hawaii.edu) was developed to make the rainfall maps, data, and related information easily accessible. The maps depict rainfall patterns by color and/or by isohyets (lines of equal rainfall). The interactive map allows users to see the patterns of mean monthly and annual rainfall and corresponding uncertainty, zoom in on areas of particular interest, navigate to specific locations with the help of a choice of different base maps, and click on any location to get the mean annual rainfall and a graph and table of mean monthly rainfall. The locations of stations can also be shown on the interactive map. Clicking on a station gives both station and mapped estimates of monthly rainfall along with station metadata.

Rainfall maps can also be downloaded in various forms. Our analysis produced digital maps called rasters or grids. On these maps, the islands are divided into 8.1-arcsecond spatial units, or approximately 234 × 250 m (770 × 820 ft). Rainfall and uncertainty are estimated for each spatial unit. GIS (Geographic Information System) users can obtain mean and uncertainty maps as raster files, as well as shapefiles of isohyet lines and station points. Alternatively, image files showing rainfall patterns by color and/or by isohyets can be downloaded.

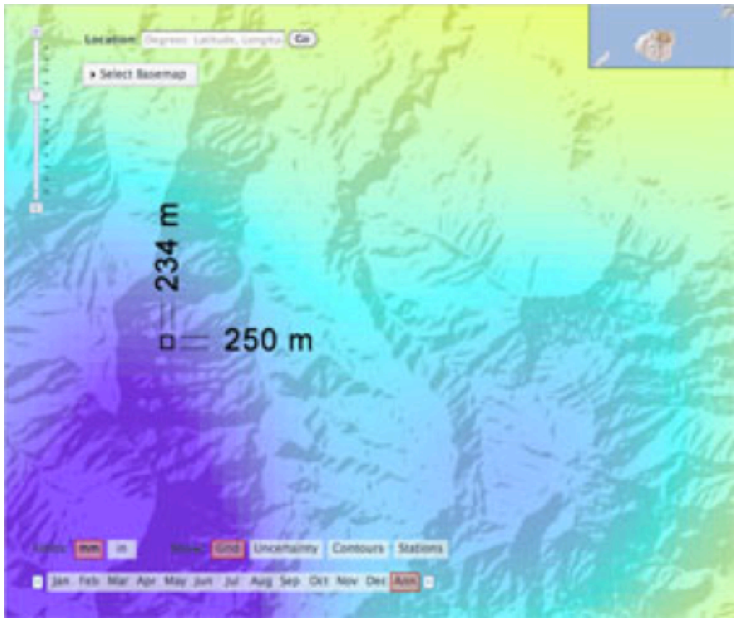

Figure 1. The spatial unit for rainfall analysis in the 2011 Rainfall Atlas of Hawai‘i is 8.1 arcseconds, or 0.00225° longitude and latitude, equivalent to about 234 m (east-west) by 250 m (north-south).

Rainfall measurements taken at over 1,000 stations were used as the principal source of information in the development of the rainfall maps. Files containing estimated mean monthly and annual rainfall and uncertainty for each station used in the analysis are available for download. A file with information on each station, including the name, observer, location, elevation, and period of record, is also available.

This report and the Rainfall Atlas of Hawai‘i website update and supersede the original Rainfall Atlas of Hawai‘i (Giambelluca et al., 1986; herein referred to as the “1986 RF Atlas”). The following pages describe the input data, explain the methods used, and examine the results of the new rainfall analysis. A more detailed description of the methodology is given in the Appendix to this report.

History of Rainfall Mapping in Hawai‘i

The earliest known rainfall observations in Hawai‘i were taken by Dr. Thomas Charles Byde Rooke in 1837 at Nu‘uanu Avenue and Beretania Street in Honolulu. By the end of the 19th century, rainfall was being monitored at 106 stations. That number increased to 422 by 1920. As data accumulated and the number of observation sites expanded, various efforts were made to map the spatial patterns

of rainfall. Table 1 lists some of the more prominent of those efforts.

With each successive analysis, the resulting maps were refined and improved, taking advantage of a growing database and better understanding of the processes controlling rainfall. Differences among these maps reflect this refinement and improvement, as well as fluctuations in rainfall over time. Figures 2-8 show some examples of analyses of monthly and annual rainfall for O‘ahu.

Table 1. Prior Rainfall Maps of Hawai‘i

Statistic	Interval	Coverage	Citation
Mean	Annual	O‘ahu	Voorhees (1929)
Mean	Annual	O‘ahu	Nakamura (1933)
Mean	Annual	Major islands	Feldwisch (1939)
Mean	Annual	Maui	Stearns & Macdonald (1942)
Median	Monthly	O‘ahu	Halstead & Leopold (1948)
Mean	Annual	East Maui	Leopold (1949)
Mean	Annual	Major islands	Stidd & Leopold (1951)
Mean	Monthly, Annual	Major islands	Mordy & Price (1955)
Median	Monthly, Annual	Major islands	Taliaferro (1959)
Mean	Annual	Major islands	Blumenstock & Price (1967)
Median	Annual	Major islands	Dept. Land & Nat. Res. (1973)
Median	Annual	Major islands	Meisner et al. (1982)
Mean, Median	Monthly, Annual	Major islands	Giambelluca et al. (1986)
Mean	Monthly, Annual	Major islands	Daly et al. (2006)

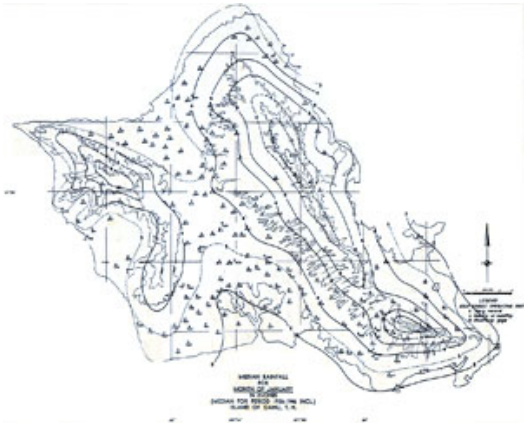

Figure 2. Map of median January rainfall for the island of O‘ahu, developed by Halstead and Leopold in 1948. The base period of the statistics is 1936–1946.

Figure 3. Map of mean January rainfall for the island of O‘ahu, developed by Mordy and Price in 1955. No common base period was used. Periods of record ranged from 10 to 68 years.

Figure 4. Map of median January rainfall for the island of O‘ahu, developed by Taliaferro in 1959. The base period of the statistics is 1933–1957.

Figure 5. Map of median annual rainfall for the island of O‘ahu, developed by Meisner et al. in 1982. The base period of the statistics is 1916–1975.

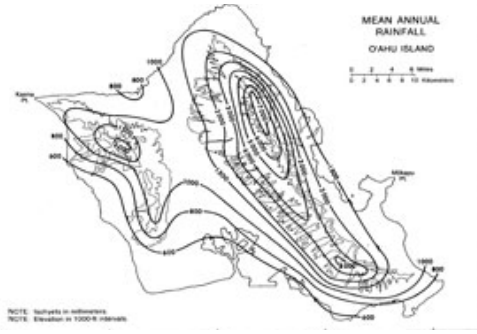

Figure 6. Map of mean annual rainfall for the island of O‘ahu from the 1986 RF Atlas developed by Giambelluca et al. The base period of the statistics is 1916–1983.

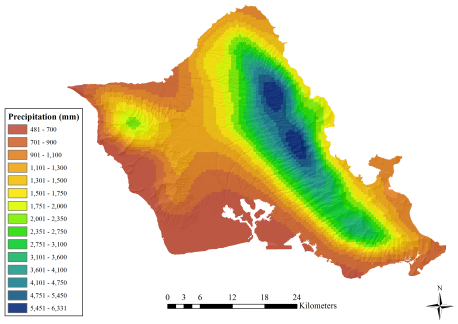

Figure 7. Map of mean annual rainfall for the island of O‘ahu, developed by the PRISM Group in 2006. The base period of the statistics is 1971–2000.

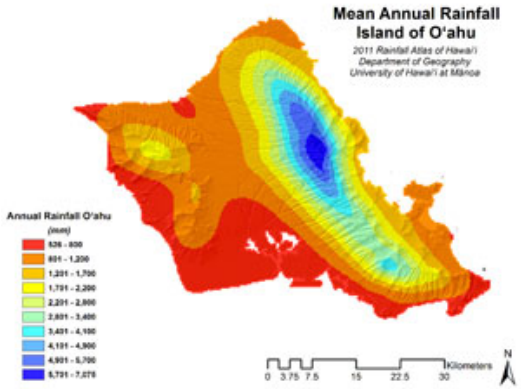

Figure 8. Map of mean annual rainfall for the island of O‘ahu, developed from the new 2011 Rainfall Atlas of Hawai‘i. The base period of the statistics is 1978–2007.

Some key differences can be seen in the methods used for these different analyses. One important issue involves the use of raingage measurements taken during different periods of time. Over the years, many gages were set up and operated for various numbers of years and subsequently discontinued. When mapping rainfall, means calculated for stations that operated during different time periods can result

in erroneous spatial patterns. This problem has been addressed in various ways. Mordy and Price (1955) acknowledged this issue, but decided not to address it. They simply used all the data available for stations with 10 years of record or more. Taliaferro (1959) calculated medians for a 25-year base period (1933–1957) “based on actual and extrapolated data”. No details were provided on the method of extrapolation. Meisner et al. (1982) adjusted rainfall medians to a common 60-year base period (1916–1975) using a statistical technique called ridge regression. In the 1986 RF Atlas, Giambelluca et al. (1986) adopted Meisner’s approach, using a base period of 1916–1983 for all islands except Moloka‘i, where a 1931–1983 base period was used. In the 2011 Rainfall Atlas of Hawai‘i, each station in the selected network was “gap-filled” using a variety of statistical techniques to produce complete or nearly complete records for a 30-yr base period, 1978–2007.

Another difference among the previous maps is in the choice of a normal statistic. The average, or mean, used in the 2011 Rainfall Atlas of Hawai‘i, was commonly used in the past. But several maps were done using the median, the value for which half the observations were higher and half lower. The mean is more meaningful for hydrological purposes, because it is related to the total amount of rainfall over the base period. The mean can be strongly influenced by a relatively few extreme values, hence, some prefer the median as a more representative measure of the central tendency of rainfall.

In most prior rainfall analyses done for Hawai‘i, point rainfall values were analyzed manually by drawing lines of equal rainfall (isohyets). In areas with a dense and well-distributed network of stations, the analyst must use expert knowledge to resolve apparent conflicts among station values to produce smooth isohyets. Similarly, in areas lacking sufficient measurements, expert knowledge is called upon to estimate the patterns based on presumed relationships between rainfall and topography or patterns of vegetation. In the 2011 Rainfall Atlas of Hawai‘i manual analysis was not used. Instead, raingage data were supplemented with other predictors, in the forms of rainfall maps derived from radar, the mesoscale meteorological model MM5, and a previously done analysis incorporating relationships with terrain (PRISM, Daly et al., 2006), and statistical techniques were used to merge these different predictors to produce the final maps.

Methods

For a detailed description of the methods used in this analysis please see the appendix to this report.

The 1986 RF Atlas was developed from rainfall observations at 1203 sites in Hawai‘i, with means and medians adjusted to a common base period, and with

isohyets (lines of equal rainfall) drawn manually to represent spatial patterns. This method utilized all the available raingage data and used expert knowledge to go from point values to spatial patterns. Despite the high number of raingages, large areas had no rainfall measurements and many still do not today. These areas are generally in remote, mountainous, wet forests, which are difficult to access for measurement. However, these areas are often among the most important in terms of water resources planning and management and ecological protection.

In the new Rainfall Atlas, raingage data and expert knowledge have been supplemented with other predictors. The following types of rainfall information were used in our analysis:

1. Updated raingage data, with means calculated for the 30-year base period 1978-2007; information available only at gage sites.

   A wealth of raingage data are available in Hawai‘i. Raingages have been operated at over 2000 sites in Hawai‘i at one time or another. These stations have been established at different times and have been operated for varying lengths of time. Because of interdecadal fluctuations in rainfall, period-of-record normals from stations operated during different time periods are influenced by temporal differences, giving rise to mapping errors. In preparing maps for the 1986 RF Atlas, this problem was addressed using a form of multiple regression to adjust station normals to a common base period. In the current analysis, we collected, tested, and corrected all available raingage data for the period 1920-2007. We then applied a range of techniques to fill the gaps in the records of as many stations as possible. For stations with no more than 3 missing values during the 1978-2007 base period, mean values were calculated from the gap-filled time series.

2. Rainfall maps for the period 1971-2000 developed by the PRISM project, derived from raingage data interpolated to a grid using topographic co-variables; information available at all grid locations; uncertainty greater in areas without gages.

   PRISM (Parameter-elevation Regressions on Independent Slopes Model) is a climate mapping model developed by Christopher Daly at Oregon State University in 1993 (Daly et al., 1994). The PRISM maps are based on the assumption that elevation is the most important factor in determining precipitation. Digital monthly precipitation maps were created for the entire US (including Hawai‘i), first for the 1961-1990 time period, then updated for the 1971-2000 period. PRISM used a total of 442 stations for Hawai‘i

(including 20 “estimated” stations), at a resolution of ~450 m (Daly et al., 2006).

3. Mean radar rainfall estimates; estimates available in areas with good radar exposure.

   The National Weather Service office at Honolulu provided radar rainfall data for the 60-month period 2004-2008. These estimates have a resolution of 1° (horizontal angle measured from each radar site) by 1 km. The level-3 data set used in this study is a derived product in which rainfall rates have been estimated from radar reflectivity measurements, using a statistical relation. We composited all existing data to produce mean estimated rainfall patterns. The data in polar coordinates for each radar site were mapped in Cartesian coordinates for this analysis.

4. Mean MM5 rainfall (Yang and Chen, 2008) estimates; available at model resolution for whole state.

   High-resolution daily experimental model forecasts over the entire state (9-km resolution), Hawai‘i Island and Maui-Moloka‘i-Lana‘i Islands (3-km resolution), O‘ahu (1.5-km resolution), and Kaua‘i (1.5-km resolution) have been operational since 2003. Model runs are initialized from the global NCEP (National Centers for Environmental Prediction, Washington, DC) model output at 0000 UTC (1400 HST) each day and run for 36-hr high-resolution forecasts. The hourly model rainfall from the 12- to 35-hr forecasts were used to represent the diurnal cycle of rainfall for each day. For this project, we compiled the model-simulated rainfall climatology for each individual island using the model output during January 1, 2004 to December 31, 2007. Mean annual and monthly high-resolution rainfall maps for each island were constructed with a 1.5-km resolution for O‘ahu and Kaua‘i and a 3-km resolution for other islands consistent with model grids.

5. Rainfall estimates derived from vegetation distribution: estimates available at locations where distinct climate-related spatial shifts in vegetation are found.

   Price et al. (2007) have used climate, substrate age, biogeographical regionalization, and patterns of human disturbance to map the patterns of vegetation in the islands. As part of that effort, moisture zones were defined, representing zones with similar water input (rainfall plus cloud water interception [CWI] or “fog drip”) minus water use (evapotranspiration, ET). Taking into consideration the possible effects of CWI and ET, the moisture

zone map was used to estimate mean rainfall at specific points in areas where rainfall measurement is insufficient. These "virtual raingages" provide only mean annual estimates. Monthly amounts were approximated by analyzing the proportion of annual rainfall occurring within each calendar month for raingage stations in the general area.

To merge this information to generate gridded fields of rainfall, we used a methodology called Bayesian data fusion (Bogaert and Fasbender, 2007). In the framework of Bayesian data fusion, each type of data provides evidence for estimating the true rainfall at a given spatial location, with a certain error associated with it. For the raingage measurements, we assume that no bias exists between the measurements and the true rainfall, but the raingage measurements at each location might have different levels of uncertainty (see "What Do We Mean By Uncertainty?" section, below). Secondary datasets (radar, MM5, and PRISM) could have different biases in addition to uncertainty. The rainfall estimation procedure was tested by comparing the mapped results for raingage locations with the means based on measurements.

In some areas lacking raingage measurements, vegetation patterns were used to make estimates of rainfall at points, thus adding "virtual raingage stations" to the rainfall database. Spatial analysis of raingage and virtual raingage data, using ordinary kriging, was done to interpolate rainfall means from irregularly located point values to a regular grid. Three predictor datasets (PRISM, radar, and MM5) provided additional estimates of the mean rainfall pattern for each month. The predictor dataset maps were each tested by comparing them against rainfall at measurement sites and virtual raingage sites. This comparison allowed us to adjust (calibrate) the PRISM, radar, and MM5 predictor data sets and to assess how closely they matched the rainfall measurements after being adjusted. How well (or poorly) the predictors matched the measurements is expressed in terms of the uncertainty. The kriging method provides an uncertainty map for the interpolated rainfall observations. The lower the uncertainty, the better the predictor. To merge the kriging, PRISM, radar, and MM5 maps, the uncertainty of each predictor was used to determine its "weight", with high weights for lower uncertainty and vice versa. In many cases, one or more of the predictor data sets failed to improve the final estimate, and were therefore not used (see Table A7 in the Appendix). By giving the greatest weight to the least uncertain predictors, we obtained the best estimate of the mean at each location. The resulting maps, therefore, are derived from the best information available for each island and each month. In this process, we were also able to assess the uncertainty of the merged estimate. In Figure 9 are sample maps of the estimated rainfall patterns and corresponding maps of uncertainty derived

from ordinary kriging interpolation and each of the predictor data sets. In this case, incorporating the radar estimate did not improve the final map, and was not used.

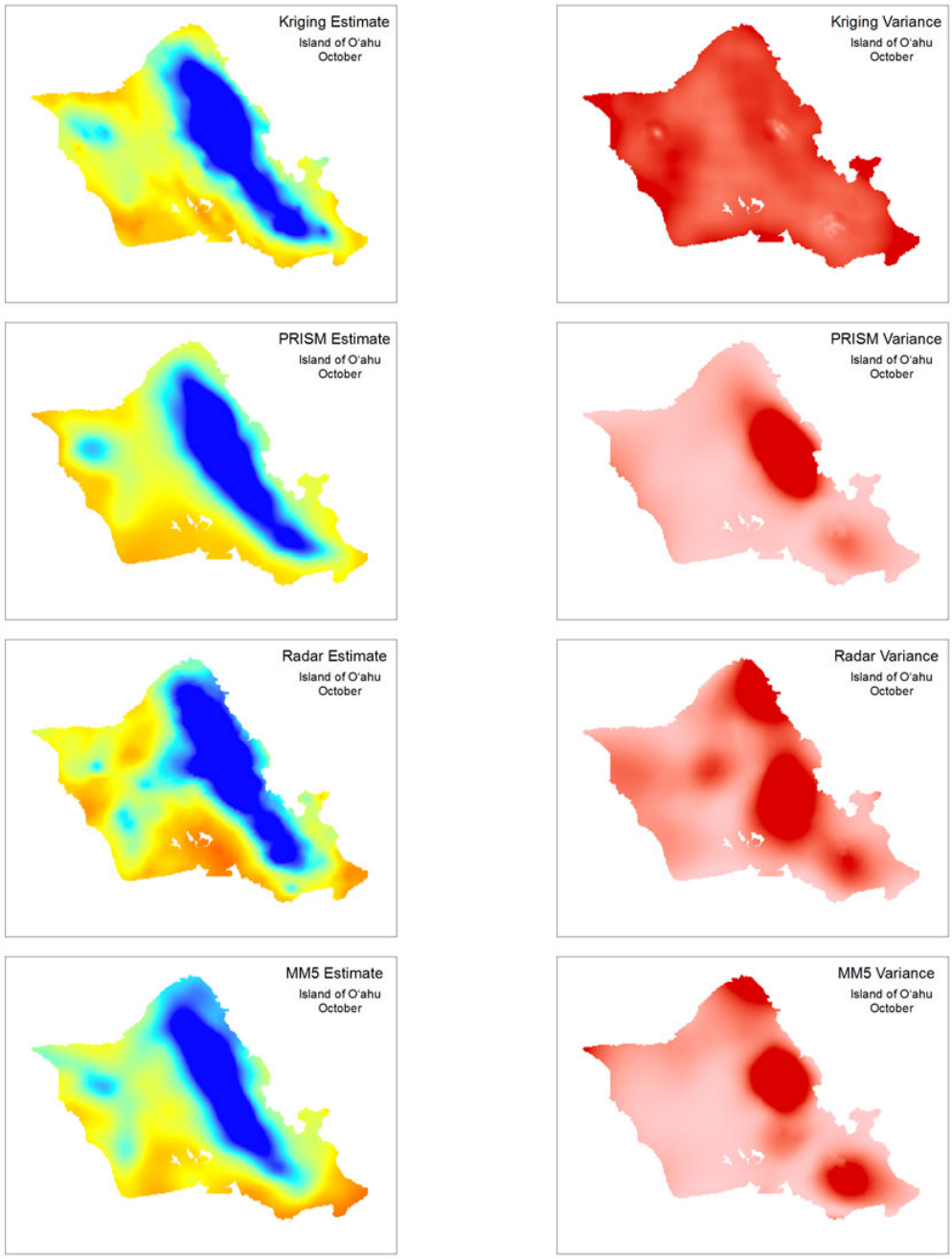

Figure 9. Maps showing the distribution of estimated mean October rainfall (left column) and the corresponding variance (uncertainty; right column) for O'ahu for the ordinary kriging interpolation and each of the three predictors.

Hawai‘i Rainfall Network

Raingage measurements form the basis of our analysis of the spatial patterns of rainfall. Because of the importance of rainfall information to agriculture, water supply, flood hazard, ecosystem health, and other interests, and because of the relative ease of measurement, rainfall has been measured in Hawai‘i at over 2,000 sites (at least 2,188 stations on record). Record lengths vary from a few months to many decades, and the majority of stations were eventually discontinued. The types of gages and the methods of recording are numerous, with manually-read daily raingages the most common overall.

The monthly rainfall database that we compiled for the 2011 Rainfall Atlas of Hawai‘i includes 1067 stations, with 517,017 station-months (43,085 station-years) of data over the period 1874-2007. These stations on average had 485 months of data (40 years of data) throughout that period, with the longest running station spanning 1426 months (119 years). The number of stations operating at any given time increased during the 19th and early 20th centuries, reaching a peak of 1030 stations in 1968. After that, the number of active stations declined, and now includes only 340 stations (Figure 10). This trend is linked to the growth and decline of plantation agriculture in Hawai‘i. Pineapple and sugarcane cultivation in Hawai‘i were carefully managed with much attention given to relevant weather observations. Sugarcane, in particular, depended on irrigation in most areas. Plantations and affiliated irrigation companies throughout the islands, therefore, maintained a large network of raingages. Most of these stations were discontinued over the past 30 years.

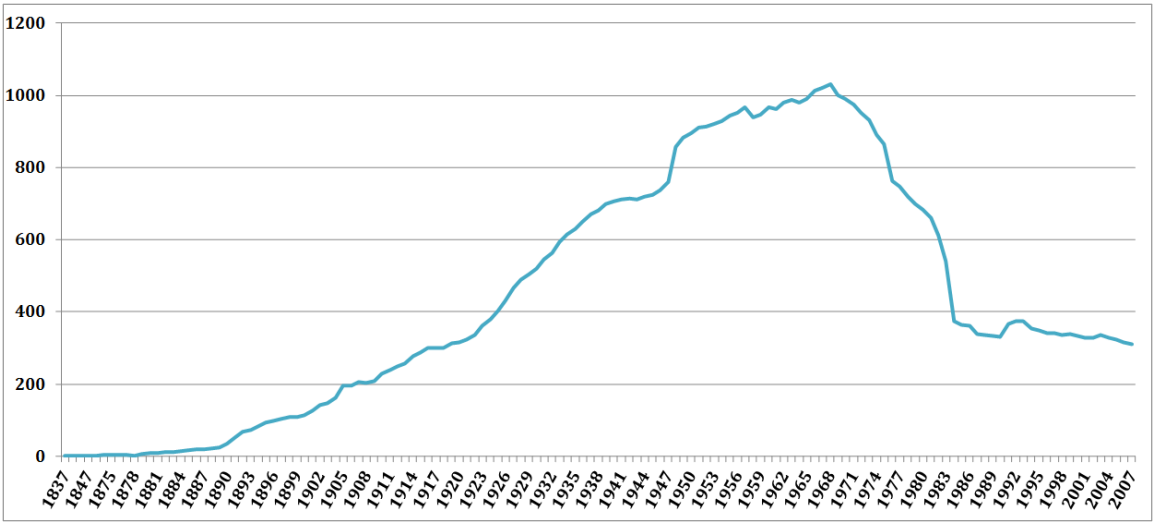

Figure 10. The number of raingage stations operating in each year.

Plantation weather records, including information on the geographical coordinates, elevation, and observer of each station, were maintained by the Pineapple Research Institute (PRI) and the Hawai‘i Sugar Planters’ Association (HSPA). Eventually, the Hawai‘i Department of Land and Natural Resources (DLNR), Division of Water and Land Development (DOWALD), predecessor of the Hawai‘i Commission on Water Resource Management, hosted the Office of the State Climatologist, where weather records from all sources were archived and processed. DOWALD maintained a set of maps on which all active and discontinued weather stations were plotted. In 1973, DLNR published a report, “Climatological Stations in Hawaii” with station information and maps of all station locations (Department of Land and Natural Resources, 1973). This report remains an important resource today. Over time, a change in the map datum used for Hawai‘i, typographical errors, and a lack of precision in the recorded station coordinates resulted many errors in the station coordinates. In developing maps of rainfall patterns, it is crucial to know the station locations with accuracy and precision. As part of the 2011 Rainfall Atlas of Hawai‘i project, we made an effort to improve estimates of station locations, and to estimate the level of uncertainty in the location of each station. To do this, we corrected for the datum shift, looked for and fixed as many typographical errors as possible, and relied heavily on DLNR Report R42 to find the most likely historical locations of hundreds of discontinued stations. Our estimates of station locations are available for download. Note that while high precision coordinates for the HydroNet stations were used in our analysis, we provide only low precision for these stations at the request of NOAA.

Hawai‘i Monthly Rainfall Database

The basis of all rainfall analyses is the database of raingage measurements. The first task in developing the 2011 Rainfall Atlas of Hawai‘i was to gather all available rainfall data for the State of Hawai‘i.

Data Sources

The real sources of raingage data are the observers who meticulously measured and recorded rainfall amounts over the past 170 years. Our proximate sources, however, were several existing datasets. To develop the monthly rainfall database, we first located and compiled all of the different Hawai‘i rainfall datasets. The largest was the State rainfall dataset, which has been maintained by the Hawai‘i Department of Land and Natural Resources and the Office of the State Climatologist. The original paper reporting sheets are archived in the State Climatologist’s office in the Meteorology Department, University of Hawai‘i at Mānoa. This dataset is comprised of rainfall measurements collected by various agencies and individuals since the

mid-1800s. Rainfall amounts were recorded by hand on a standard form, and carbon copies were mailed to several locations, including the Office of the State Climatologist. Some of these records were eventually entered into digital databases. The most recent update of the Hawai‘i digital monthly database was done in the mid-1980s. We entered data for stations with hard-copy data records during the intervening years.

The next largest source of rainfall data was from the National Climatic Data Center (NCDC). We obtained both the monthly and daily datasets for the islands. Records for most of this dataset were derived from a portion of the same original paper records as the State dataset. Daily values were summed to get monthly totals. When we compared the NCDC daily, NCDC monthly, the State digital dataset, and the original paper records, the NCDC monthly values were usually found to match the State digital and paper values, and the daily values often were not. Therefore, the NCDC daily dataset was deemed unreliable and not used in our analysis.

Another contributor of rainfall data was the U.S. Geological Survey (USGS). The data for Hawai‘i were downloaded from the USGS website in daily format, and converted to monthly totals.

A number of smaller raingage networks were also included in the dataset. Most of these stations did not begin operating until the 1980s or later, but they were very important additions to the dataset because of their locations and high data quality. One of these networks, HydroNet, is run by the National Weather Service. Another important small network, RAWS (Remote Automated Weather Stations), is operated by the National Interagency Fire Center (NIFC), with the data posted by the Western Regional Climate Center (WRCC). The HaleNet dataset, derived from a network of climate stations on Haleakalā, Maui was included. Data from SCAN (Soil Climate Analysis Network, a network run by the US Department of Agriculture (USDA) Natural Resources Conservation Service (NRCS) National Water and Climate Center) on the Island of Hawai’i, were available, but were not incorporated because of the brevity of their data records. Most of these stations were established in 2005, and therefore had only three years of data in the 30-year base period used to calculate means for the 2011 Rainfall Atlas of Hawai‘i.

State Key Numbers

The State Key Number (SKN) system was devised many decades ago as a system of unique identification numbers for all weather stations in Hawai‘i. Numbering is organized by island with these ranges:

Hawaii:	1.00	–	223.00
Maui:	248.00	–	497.00
Kahoolawe:	499.00	–	499.99
Molokai:	500.00	–	599.00
Lanai:	650.00	–	696.00
Oahu:	700.00	–	914.00
Kauai:	925.00	–	1147.00
Niihau:	1150.00	–	1150.99

The numbers within each island tend to be clustered by location, and related or closely located gages often have a decimal added that follows this order: 830.00, 830.10, 830.20, 830.30… 830.90, 830.11, 830.12…

All of the stations from the State, NCDC, and USGS databases had already been assigned State Key Numbers, although NCDC uses its own numbering system and does not use the State Key Number to identify stations. Stations from the smaller networks had not yet been assigned SKNs. All stations without a SKN were plotted along with the existing stations, and the ranges of its neighbors were recorded to find an appropriate new (unused) number. We then recommended new SKNs to the State Climatologist, who approved them.

Gap-Filling

Over the years, many gages were set up and operated for various numbers of years and subsequently discontinued. Because rainfall can vary significantly on time scales of years to decades, the “era” of a particular gage, i.e., the time during which it operated, can have a big influence on the estimated mean rainfall. When mapping rainfall, means calculated from different eras can produce spurious spatial patterns. This problem has been addressed in previous efforts to map Hawai‘i rainfall by using various methods to adjust normals to a common base period.

In the 2011 Rainfall Atlas of Hawai‘i, we chose to fill gaps in the records of as many raingages as possible. Being able to fill the gaps in the data record allowed us to compute base period means for a much larger number of stations, thereby improving the spatial coverage. Figure 11 illustrates the potential to improve the spatial coverage of point rainfall estimates by gap-filling the records of stations that operated before or after the period of interest.

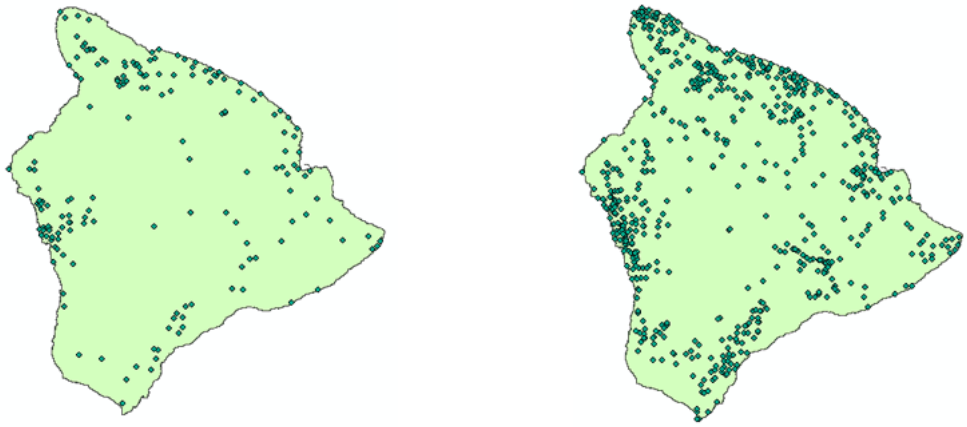

Figure 11. Maps showing the locations of raingage the stations on the Island of Hawai‘i that reported data in 1980 (left) and the locations of all of the stations that ever recorded data on the Island of Hawai‘i (right).

We used a variety of methods to fill gaps. In general, statistical relationships between rainfall at nearby stations are established during periods when stations had concurrent data. Subsequently, these relationships can be used to estimate rainfall at one station (with missing records) based on active station(s). Details of this approach can be found in the appendix to this report.

Base Period Selection

Before calculating station monthly and annual mean rainfall, it was necessary to decide upon a common base period for averaging the records. In previous Hawai‘i rainfall analyses, a number of different averaging periods were used. The 1986 RF Atlas used the period 1916–1983 (68 years) for all islands except Moloka‘i, where 1931–1983 (53 years) was used. The length of the averaging period is the first question. Using a long period does a better job of averaging out the effects of slowly changing natural cycles, such as the Pacific Decadal Oscillation (PDO). On the other hand, because Hawai‘i is experiencing a long-term downward trend in rainfall, using a shorter averaging period may be better for characterizing the current and near future situation. The National Ocean and Atmospheric Administration (NOAA) uses a standard 30-year averaging period, with statistics updated at the end of each decade. Considering all these issues, and giving more weight to the recognition of the long-term trend in rainfall, we opted for a 30-year averaging period. We chose to use 1978–2007, which was the most recent 30-year period for which a high percentage of data for active stations were available as of the start of the project. We acknowledge that for most of this period, the PDO was in its positive phase, which is generally associated with lower rainfall.

What Do We Mean by Uncertainty?

The station means and maps of mean monthly and annual rainfall represent our best estimates for the 30-year base period 1978–2007. However, for many reasons, it is not possible to determine the exact value of mean rainfall for any location, even at the stations. In recognition of that, we provide estimates of the uncertainty in our estimates of station means and mapped means.

The uncertainty value that we provide can be interpreted as a plus-or-minus range around the estimated mean. While we cannot say exactly what the mean is, we are confident that it lies within that range. For example, mean annual rainfall for the US Geological Survey's Moanalua station (State Key Number 772.3) has an estimated mean annual rainfall of 3317 mm (130.6 inches) and an uncertainty of 128 mm (5.0 inches). That means the true mean annual rainfall for the base period is likely to be between 3189 and 3445 mm (125.6 and 135.6 inches). The uncertainty statistic we use is in the form of a standard deviation. If we assume the sample of possible estimated means has a normal ("bell-shaped") distribution, then the likelihood of the true value being within ±1 standard deviations from the mean is about 68%.

Many different things influence the level of uncertainty, and only some of them can be evaluated in a systematic way. In the case of the station means, we considered three sources of uncertainty, and ignored other sources, such measurement errors, which cannot be readily quantified. Of those we considered, the first is related to the number of values used to calculate the 30-year mean. We included stations with up to three missing values within the 30-year base period. But, we realize that the more missing values we have the more uncertain the resulting mean is. For each station with less than 30 years of data, we calculated the added uncertainty of each missing value and multiplied it by the number of missing values. The second source of uncertainty is related to the gap-filling process. Wherever possible, we made estimates of monthly rainfall to fill gaps in the records of stations. This was used to fill gaps within the period of record, such as when a gage was malfunctioning, and to fill periods before and/or after the gage operated. As a result, the 1978–2007 mean for a given station could have anywhere from 0 to 30 estimated (as opposed to measured) values. Gap-filling is essential for producing means that pertain to a common base period, and allows us to use a much larger number of stations than we would otherwise. But, obviously, an estimated monthly rainfall total is more uncertain than a measured one. We calculated estimated values at all stations for all months, even those with measurements. This was done to allow us to compare the estimates with measurements to obtain a measure of the uncertainty of the estimates at each station. This value was then multiplied by the number of estimated values to get the uncertainty resulting from gap filling. The third source of

error was related to the station locations. In compiling the data set used in this analysis, we found that many errors existed in the published locations. Poor precision, conflicting information about station coordinates, use of an obsolete map datum, typos, and other problems led to many stations being out of place on our maps. Some were even well out in the ocean. We worked hard to eliminate these problems, but were still unsure about the locations of stations, especially ones that had been long discontinued. Imprecision in the station location amounts to an uncertainty in the rainfall. Consider that in some areas, the rainfall gradient is so steep, a station misplaced by only 1 km (0.6 miles) could misrepresent actual mean rainfall by 1500 mm (59 inches). We estimated uncertainty in the location of each station, applied it to the local rainfall gradient to estimate uncertainty in rainfall resulting from uncertainty in the station location. The uncertainties from these three sources were combined to give the total uncertainty in each station mean.

Uncertainty in mapped rainfall results from the combined uncertainty of the interpolated station values, derived using a technique known as ordinary kriging, and the uncertainty in all of the predictor data used to produce the map. In general, interpolation uncertainty is low near stations and increases as the distance to the nearest station increases. In other words, uncertainty is greatest where there are no nearby stations. The spatial patterns of uncertainty in radar-estimated rainfall, the MM5-estimated rainfall, and rainfall taken from the PRISM analysis, were estimated by comparing the mapped values with station values. When merging the predictor maps to get the final estimate at each location, the uncertainties in the predictors were also combined to get a map of total uncertainty at each location.

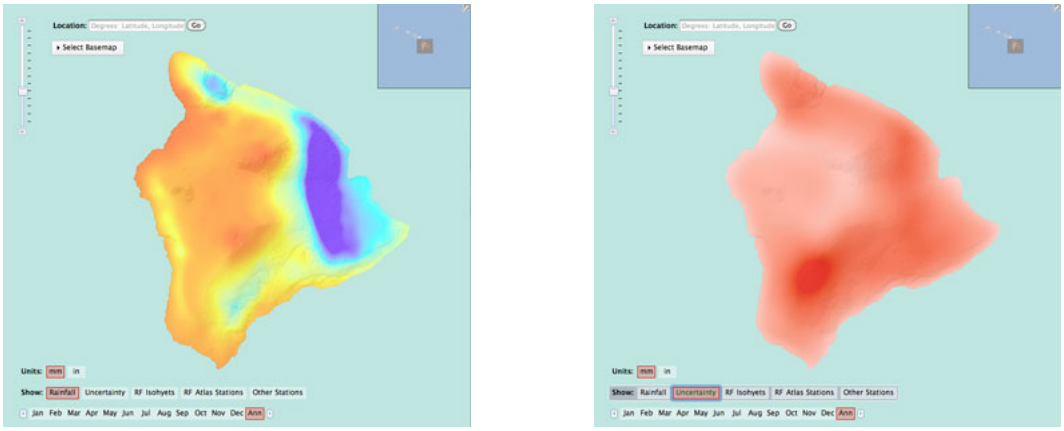

Figure 12. Map of mean annual rainfall (left) and the corresponding uncertainty map (right).

The rainfall map in Figure 12 shows the high rainfall area (blue) along the windward slopes of Mauna Kea and Mauna Loa above Hilo, the local rainfall peaks (yellow and blue) on windward Kohala, near Pāhala in Ka‘u District along the southeastern flank of Mauna Loa, and along the slopes above the Kona coast. Dry areas (orange to red) are seen at the Mauna Kea and Mauna Loa summits and along the leeward coasts. In the map on the right side of Figure 12, showing the uncertainty expressed as a standard deviation, high rainfall areas tend to have higher uncertainty (darker). However, estimated rainfall is most uncertain along the southwest rift of Mauna Loa. This suggests that the available raingage data coverage is sparse and the quality of the predictor sets is lower in that area than other areas. One should take the level of uncertainty into consideration when making any use of the mapped rainfall estimates.

Testing

We tested the resulting fused maps by comparing station monthly means with mapped monthly means. Figure 13 shows a scatterplot of paired station and map values. As can be seen from the figure, the maps faithfully represent the station means with a small amount of scatter about the best-fit line, and minimal bias. The scatter is produced when a station mean is in conflict with the estimates from predictor variables and/or the means of nearby stations. While the station means are the best source of information for mapping rainfall, they are not perfect. As previously described, station means are subject to uncertainty resulting from measurement error, gap-filling, small sample, and location error. In recognition of this uncertainty, we do not force the map to reproduce the station mean precisely, especially when other information suggests a different value.

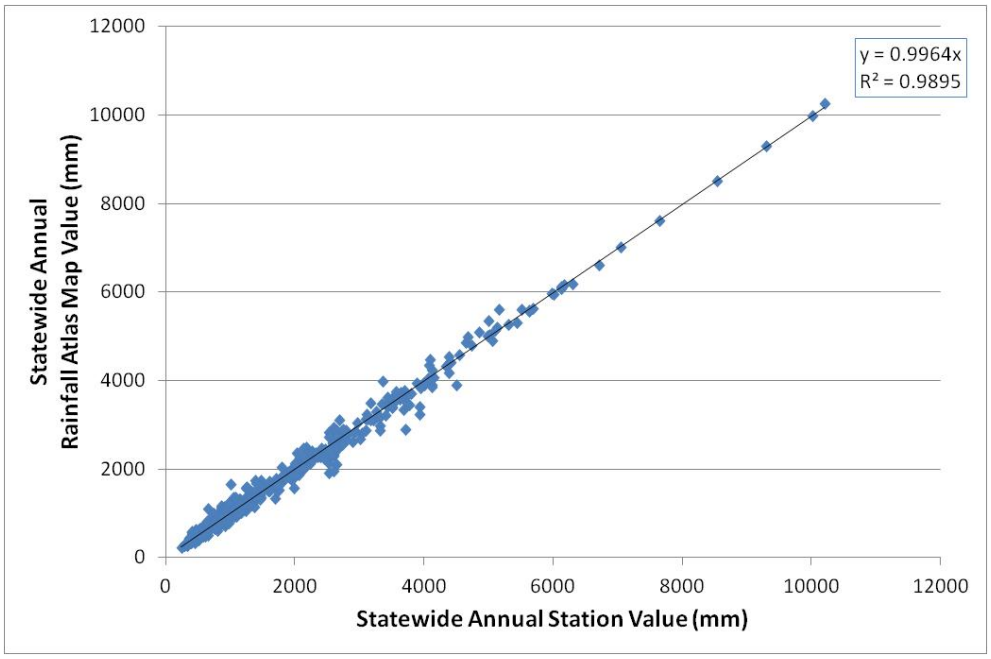

Figure 13. Scatterplot of station mean annual rainfall versus mapped mean annual rainfall.

References

Bogaert, P. and D. Fasbender, 2007. Bayesian data fusion in a spatial prediction context: a general formulation. *Stoch. Environ. Res. Risk Assess.*, 21: 695–709.

Blumenstock, D.I. and Price, S. 1967. Climate of Hawaii. In Climates of the States, no. 60-51, Climatography of the United States, U.S. Department of Commerce.

Daly, C., Neilson, R.P., and Phillips, D.L. 1994. A statistical-topographic model for mapping climatological precipitation over mountainous terrain. *Journal of Applied Meteorology* 33: 140-158.

Daly, C., Smith, J., Doggett, M., Halbleib, M., and Gibson, W. 2006. High-resolution climate maps for the Pacific Basin Islands, 1971-2000. Report submitted to National Park Service Pacific West Regional Office. PRISM Group, Oregon State University. http://www.botany.hawaii.edu/basch/uhnpscesu/pdfs/sam/Daly2006AS.pdf

Department of Land and Natural Resources. 1973. Climatological stations in Hawaii. Report R42, Division of Water and Land Development, DLNR, State of Hawai‘i. 187 pp.

Feldwisch, W.F. 1939. Progress report (1939)--Water resources. Territorial Planning Board, Territory of Hawai‘i, Honolulu.

Giambelluca, T.W., Nullet, M.A., and Schroeder, T.A. 1986. Rainfall Atlas of Hawai‘i, Report R76, Hawai‘i Division of Water and Land Development, Department of Land and Natural Resources, Honolulu. vi + 267 p.

Halstead, M.H. and Leopold, L.B. 1948. Monthly median rainfall maps, what they are—how to use them. Report No. 2, Meteorology Department, Pineapple Research Institute and Hawaiian Sugar Planters' Association. 18 pp.

Leopold, L.B. 1949. Average annual rainfall of East Maui, T.H. *Hawaii Sugar Planters' Record* 53(2): 47-59.

Meisner, B.N., Schroeder, T.A., and Ramage, C.S. 1982. Median rainfall, State of Hawaii. Circular C88, Division of Water and Land Development, Department of Land and Natural Resources, State of Hawai‘i.

Mordy, W.A. and Price, S. 1955. Average monthly rainfall maps. Meteorology Department, Pineapple Research Institute, and Experiment Station, Hawaiian Sugar Planters' Association.

Nakamura, W.T. 1933. A study of the variation in annual rainfall of Oahu Island (Hawaiian Islands) based on the law of probabilities. *Monthly Weather Review* 61: 354-360.

Price, J., Gon III, S.M., Jacobi, J.D., Matsuwaki, D. 2007. Mapping plant species ranges in the Hawaiian Islands: developing a methodology and associated GIS layers. Hawai‘i Cooperative Studies Unit Technical Report HCSU-008. University of Hawai‘i at Hilo, Hilo, Hawai‘i.

Stearns, H.T. and Macdonald, G.A. 1942. Geology and ground-water resources of the island of Maui, Hawaii. Bulletin 7, Hawaii Division of Hydrography. 344 pp.

Stidd, C.K. and Leopold, L.B. 1951. The geographic distribution of average monthly rainfall, Hawaii. On the rainfall of Hawaii, a group of contributions. *Meteorological Monographs* 1(3): 24-33.

Taliaferro, W.J. 1959. Rainfall of the Hawaiian Islands. Hawaii Water Authority, State of Hawai‘i, Honolulu. 396 pp.

Voorhees, J.F. 1929. A quantitative study of rainfall of the island of Oahu. App. A, Report of the Honolulu Sewer and Water Commission to the Legislature of the Territory of Hawai‘i, 15th Regular Session.

Yang, Y., and Y.-L. Chen. 2008. Effects of terrain heights and sizes on island-scale circulations and rainfall for the island of Hawaii during HaRP. *Monthly Weather Review* 136: 120-146.

APPENDIX
Rainfall Atlas of Hawai‘i—Detailed Methodology
Appendix to The Rainfall Atlas of Hawai‘i 2011 Final Report

Thomas W. Giambelluca, Qi Chen, Abby G. Frazier, Jonathan P. Price
Yi-Leng Chen, Pao-Shin Chu, and Jon K. Eischeid

October 2011

Database Development

Collecting Sources

State Rainfall Dataset. The first step in developing the monthly rainfall dataset needed for the development of the new rainfall atlas maps was to locate all of the different sources of data. The largest set of rainfall data came from a dataset maintained by the State of Hawai‘i, based on original data reporting sheets now housed in the State Climatologist’s office, Department of Meteorology, University of Hawai‘i at Mānoa. These data are derived from measurements collected by various individuals and organizations since the mid 1800s. Rainfall amounts were recorded by hand on a standard form, and carbon copies were mailed to a central location where they were eventually entered into a digital database. Hand recording of data, transferring data to summary sheets, adding monthly sums, and computer data entry created opportunities for errors to have crept into the dataset. Therefore, thorough data quality control measures were required.

The data were carefully screened for outliers due to obvious typographical errors, as well as other inconsistencies including cases in which the same year was entered twice for a given station (sometimes with different data), and some instances of identical data for two different stations for multiple years. Some data were flagged as suspicious by the people who performed the data entry, and these were checked against the original paper reporting sheets to resolve conflicts. A few station months had rainfall totals of 100 inches or more, which were coded as “9998” instead of the actual amount, due to data field length limits at the time of the original data entry. In those cases, we went to the paper records to get the actual measured amount. Any station that was marked in the station metadata as “accumulated”, i.e., read at a frequency of less than once per day with the multi-day total recorded, was also screened, and any totals accumulated over more than 1 month were removed from the dataset. All stations that recorded zero rainfall in a given month were examined. Data from stations with high numbers of zero-rain months in very wet areas were deemed likely to have been recorded as accumulated totals from

infrequent readings, especially if the zero months are followed by a very large rainfall total.

National Climactic Data Center. The next largest source of rainfall data was from the National Climactic Data Center (NCDC). Monthly and daily datasets for the islands were obtained and the data were screened in a similar manner to the State dataset. The daily values had to be converted into monthly values. If the month had less than 25 daily values, it was considered missing. The two datasets were compiled and maintained separately, such that some stations in each dataset were not present in the other one. However, a large number of stations did appear in both the monthly and daily datasets. Comparing the monthly totals from the two datasets, we found that many stations had conflicting data. Some of the discrepancies were very small and attributable to rounding. However, in many cases, no obvious explanation was found for the errors. Many of these stations were also present in the State database, enabling us to crosscheck the monthly totals against the original data sheets. When comparing the values for the stations identified as having discrepancies, the NCDC monthly values were found to match State digital and paper datasets, while monthly totals derived from the NCDC daily dataset were in error the majority of the time. Therefore, the NCDC daily dataset was deemed unreliable not used in our analysis.

US Geological Survey. Another important source of rainfall data was the U.S. Geological Survey (USGS). The data for Hawai‘i were downloaded from the USGS website in daily format, and converted to monthly totals. Again, a threshold of 25 days was set as the minimum necessary for estimating the monthly total. Because these data are derived from recording raingages, we assumed that rainfall from missing days was not included (accumulated) in subsequent daily totals. For months with missing data, the monthly total was estimated using the per-day average from the days with valid observations times the number of days in the month.

Small Networks. A number of smaller raingage networks were used to supplement the dataset. Most of the stations from these networks did not begin operating until the 1980s or later, but they were very important additions to the dataset based on their locations and the high quality of these newer gages. One of these networks is run by the National Weather Service and is known as HydroNet. Another important small network that was used is known as RAWS (Remote Automated Weather Stations) and is operated by the National Interagency Fire Center (NIFC), with the data posted by the WRCC (Western Regional Climate Center). These are not the same stations that are posted by the WRCC as “Coop Sites” – the “Coop Sites” are a subset of the NCDC monthly dataset, and therefore did not need to be added. The RAWS stations in Hawai‘i are part of a larger nationwide network consisting of about 1,850 stations throughout the US. HaleNet, a network of climate stations on

Haleakalā volcano, Maui, was added to our database. These stations were first put in place in 1988 to support various research activities. Data from SCAN (Soil Climate Analysis Network – a network run by the US Department of Agriculture (USDA) Natural Resources Conservation Service (NRCS) National Water and Climate Center) on the island of Hawai‘i were not incorporated because of the brevity of their data records. Most of these stations were established in 2005, and therefore had only three years of data within the 30-year base period used in the Rainfall Atlas.

Merging Data

Assigning State Key Numbers. After all the data were collected, they were merged into one database. The first step was to ensure that all stations have a unique identifier, known in Hawai‘i as a State Key Number (SKN), assigned in ranges by island (Table A1).

Table A1. State Key Numbers by island

Island	State Key Number Range		
Hawai‘i	1.00	–	223.00
Maui	248.00	–	497.00
Kaho‘olawe	499.00	–	499.99
Moloka‘i	500.00	–	599.00
Lāna‘i	650.00	–	696.00
O‘ahu	700.00	–	914.00
Kaua‘i	925.00	–	1147.0
Ni‘ihau	1150.0	–	1150.9

The numbers tend to be clustered by location, and related gages use a decimal that follows this order: 830.00, 830.10, 830.20, 830.30… 830.90, 830.11, 830.12…

All of the stations from the State and USGS datasets had already been assigned SKNs. The stations from NCDC also had SKNs, although NCDC does not use this number to identify their stations. Station names, geographical coordinates and elevations were used to ascertain the SKNs for the NCDC stations. Most stations from the smaller networks had not been assigned SKNs. Stations without a SKN were plotted along with the existing stations, and the ranges of its neighbors were recorded to find an appropriate new (unused) number. We recommended new SKNs to the State Climatologist, who approved them.

Resolving Overlapping Data. Since the most NCDC and State data came from the same source originally, much of their data overlapped. There were also some overlaps with the smaller networks. While the majority of the overlapping periods had identical data, some discrepancies were found. In such cases, the priority was given first to the smaller networks (since the majority of these were collected

automatically and were not subject to as many human errors), second to the NCDC dataset (which had undergone data quality control), and lastly to the State dataset. A matrix was maintained with the final dataset to keep track of the source of each data value. In the final database, State data accounted for about 54% of the data, overlapping (identical) State and NCDC data made up 34%, NCDC-only was 9%, HydroNet around 2%, USGS around 1%, and the others each less than 1%.

Testing for Homogeneity

Temporal homogeneity in a data record is an important requirement of climate data. A climate data time series can contain fluctuations that are not due to real variation in the element being observed. Changes in exposure, station location, instrumentation, and observing practices can cause inhomogeneities, such as sharp discontinuities (changepoints) or gradual shifts over time. Such changes are usually not well documented in the station metadata, and are difficult to detect because they are masked by real variations. These inhomogeneities cause a bias in the time series and need to be identified and removed.

We used the Penalized Maximal *t* Test (PMT) (Wang et al., 2007) to detect inhomogeneities in the Hawai‘i rainfall data. This method tests each station against a reference series to detect changepoints. The reference series was created by averaging the best long-term stations on each island. When a changepoint was discovered, one of three actions was taken: the entire station record was deleted, the data before (or after) the changepoint year was deleted, or the changepoint was ignored and the station was left alone. A total of 59 stations were identified as having a changepoint using $p = 0.9999$. Each station with an identified inhomogeneity was compared with nearby stations to determine if one of the periods (before or after the changepoint year) aligned better with its neighbors. For example, in the case of station 493.00 shown in Figure A1, the period before 1927 was deleted because it was not consistent with the data from the nearby stations. It was assumed that this station had been moved from another (unknown) location, and the post-1927 data were consistent with the geographical coordinates recorded for the station.

Filling Data Gaps

Over the years, many gages were set up and operated for various numbers of years and subsequently discontinued. Because rainfall can vary significantly on time scales of years to decades, the “era” of a particular gage, i.e., the time during which it operated, can have a big influence on the estimated mean rainfall. When mapping rainfall, means calculated from different eras can produce spurious spatial patterns.

This problem has been addressed in previous efforts to map Hawai‘i rainfall by using various methods to adjust normals to a common base period.

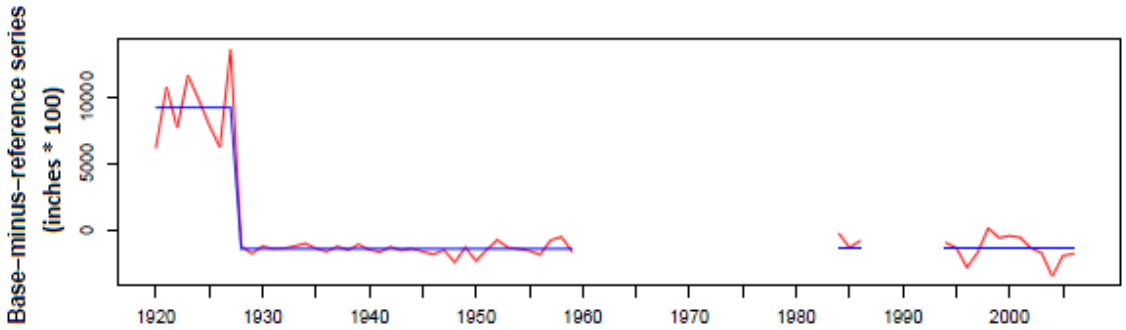

Figure A1. Homogeneity results for station 493.00. A changepoint was detected in 1927. Data before the changepoint were inconsistent with those of other stations in the surrounding area, and were deleted. Data after the changepoint were retained.

In the 2011 Rainfall Atlas of Hawai‘i, we chose to fill gaps in the records of as many raingages as possible. Being able to fill the gaps in the data record allowed us to compute base period means for a much larger number of stations, thereby improving the spatial coverage. Figure A2 illustrates the potential to improve the spatial coverage of point rainfall estimates by gap-filling the records of stations that operated only during the time before or after the period of interest.

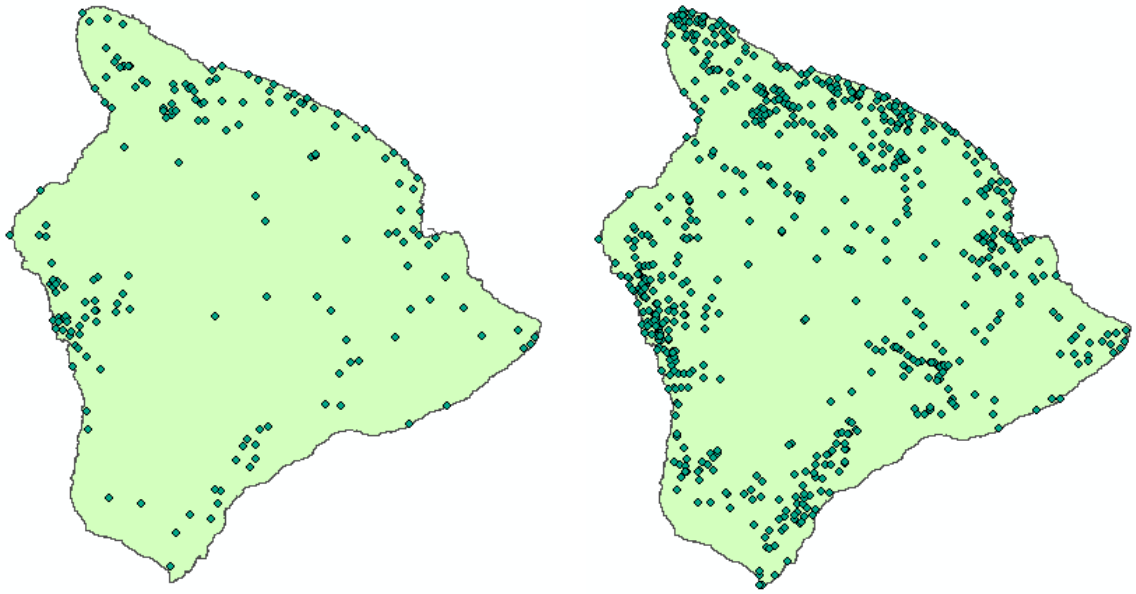

1980 Only *All Years*

Figure A2. Maps showing the locations of raingage stations on the Island of Hawai‘i that reported data in 1980 (left) and the locations of all of the stations that ever recorded data on the Island of Hawai‘i (right).

We used a variety of methods to fill gaps. In general, statistical relationships between rainfall at the station of interest and rainfall measured at nearby stations are established during periods when stations had concurrent data. Subsequently, these relationships were used to estimate rainfall at the station with missing records based on rainfall at the neighboring station(s).

Eischeid Method. Eischeid et al. (2000) developed a suite of methods to fill data gaps and create a serially complete dataset of daily temperature and precipitation for the Western United States. This method was adopted for the Hawaiian Islands monthly precipitation database to fill as many stations as possible for the period 1920-2007. For most stations, this meant extrapolating outside of the original observation period. For each missing station-month, rainfall was estimated using the best method from the following prioritized list:

1. MLAD – Multiple regression, using Least Absolute Deviations criterion
2. r^2 – Ordinary least-squares regression
3. SBE – Single Best Estimator
4. IDW – Inverse Distance Weighted
5. Average– Average of MLAD, r^2, SBE, and IDW methods

To use a given method, certain criteria have to be met. In cases where they are not met, the next best method is considered. Only stations with at least of 20 years of data were gap filled using the Eischeid approach. In the final serially complete dataset, about 30% were filled by MLAD, 16% by the r^2 method, 12% by SBE, 27% by IDW, and 15% by the Average method. Figure A3 shows an example of a station filled through the Eischeid method.

Normal Ratio Method. By using only stations with at least 20 years of observed data, the rainfall network was noticeably diminished. Figure A4 shows the spatial coverage of the gages with at least 20 years of observed data compared to the network of gages with less than 20 years of original data. Many important areas have only stations with less than 20 years of data. In order to rescue these shorter record stations, a different method was used to fill the missing years. Although these stations did not have enough data to establish a robust regression necessary for filling using the Eischeid method, the simpler Normal Ratio method was successful. We used this method to gap-fill the records of stations with less than 20 years of data, but with at least 80 months of data during the 30-year based period (1978-2007).

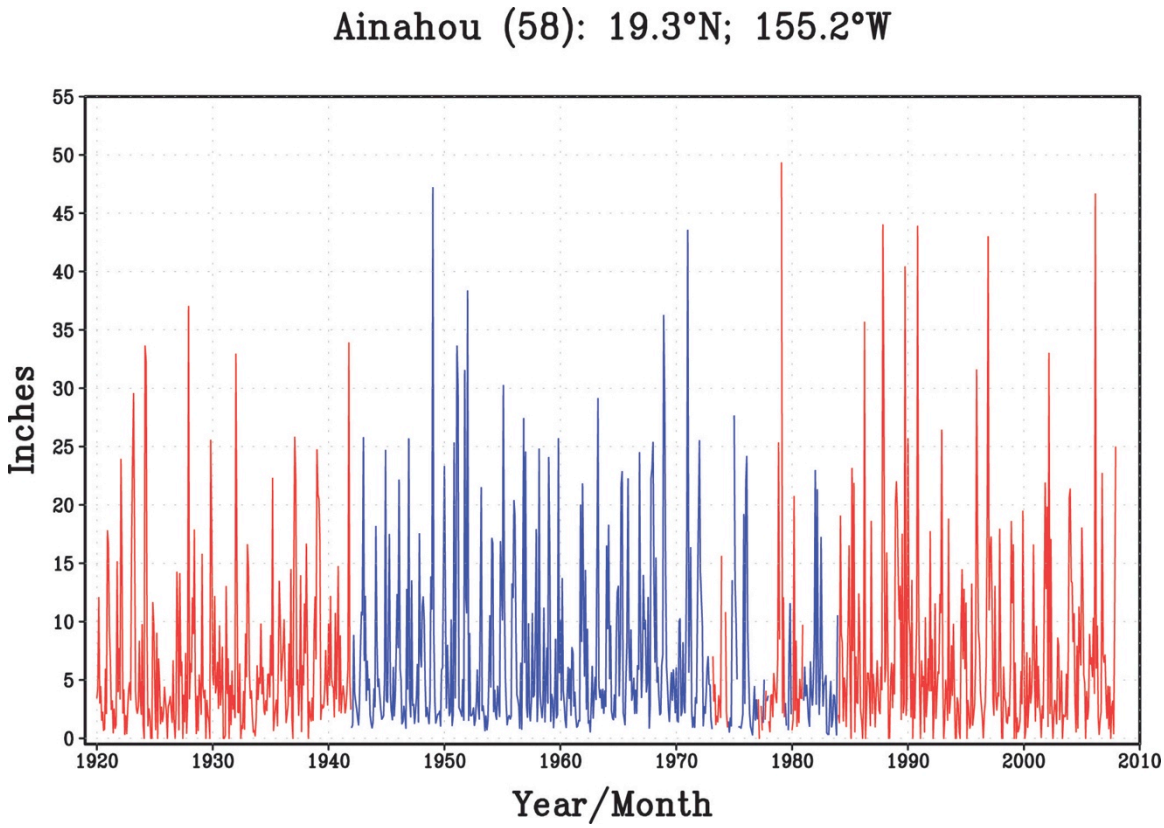

Figure A3. Station 58.00 filled by Eischeid method. Blue lines are original (observed) data, red lines are filled data. Gaps were filled within the original period of record, and extrapolated out to complete the time series from 1920-2007.

The normal ratio method (Paulhus & Kohler, 1952) uses the ratios of the mean of the station in question to the means of the most well correlated stations as weights in the estimation procedure:

$$P_x = \frac{1}{n}\left(\sum_{i=1}^{n} P_i \frac{N_x}{N_i}\right) \quad (1)$$

where, *Px* = predicted rainfall at station x, *Nx* = average rainfall at station x, *Ni* = average rainfall at i^{th}-best correlated station, and *Pi* = rainfall at i^{th}-best correlated station.

In our application of this approach, the four most highly correlated stations (regardless of island) for each station were used. A minimum correlation (r) of 0.88 was set as the minimum for a predictor station, and the ratios were computed for the overlapping period of data between the stations. A minimum of 5 overlapping years was required in a given month. If the ratio was greater than 2.5 or less than 0.5, it was not used.

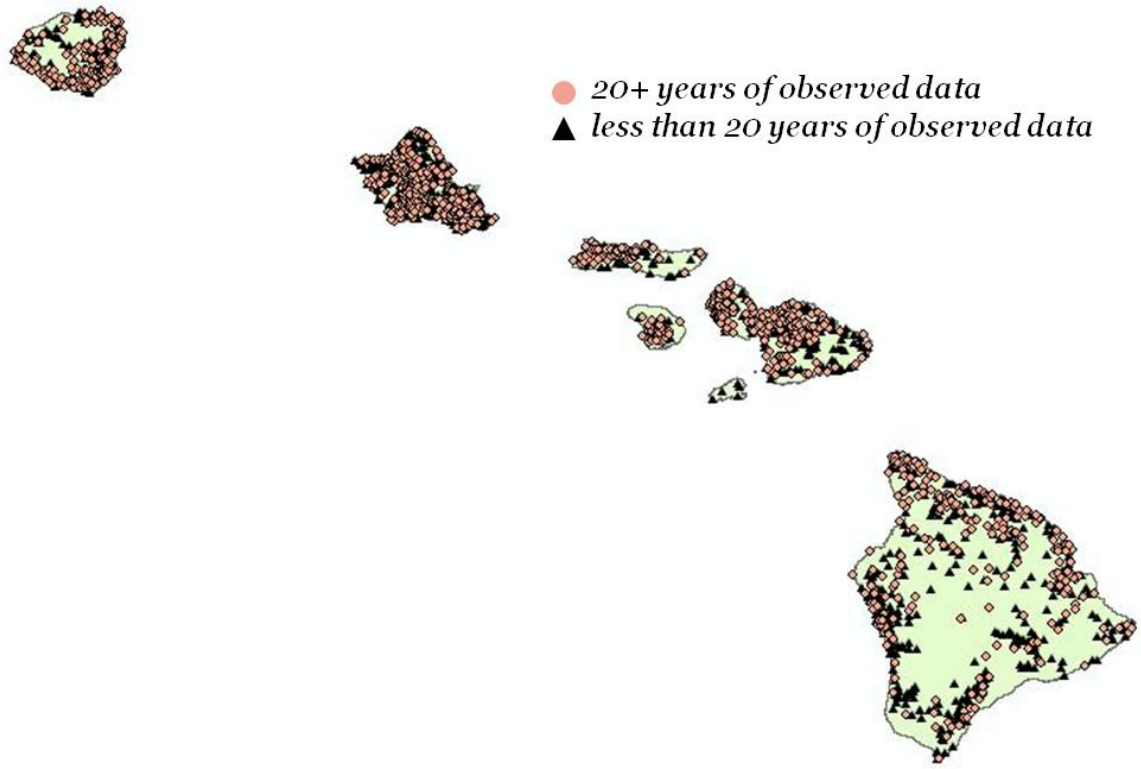

Figure A4: A map of the rainfall stations on the main Hawaiian Islands, differentiated based on the record length of original data.

Conducting Quality Control Testing of Gap-Filled Data

Bias and RMSE. With the gaps in the dataset filled, quality control was performed to ensure that the filled data were consistent with the original data for each station. For the purposes of testing the results, the gap-filling methods were also used to estimate rainfall for all months with actual observations. This allowed us to compute bias and root mean square (RMSE) statistics for each station month.

The bias was computed by taking the mean of the deviation between original and filled values for each station-month. Both bias and RMSE were expressed in relative terms by dividing each by the mean rainfall (using original rainfall values only) for the station-month. Any station-months with bias > |1| and an RMSE > 2 were flagged as suspicious. During the next quality control step using quantile standardizations, all of the station months that were identified by the bias and RMSE criteria were identified again, which gave confidence in the choice to remove the filled data from those station months. Using the bias 41 more station months were identified to remove, and based on RMSE, filled data from 28 more station months were removed.

Extremes. Errors in estimated data often manifest themselves in the frequency distribution, especially in the number of occurrences at the extremes. We implemented a procedure to identify poor filled data based on the tails of the frequency distribution. To examine the right side of the distribution, the ratio R was calculated for each monthly data value:

$$R_{s,m,y} = \frac{x_{s,m,y} - x(1/2)_{s,m}}{x(5/6)_{s,m} - x(1/2)_{s,m}} \quad (2)$$

where x = an individual monthly filled or original rainfall value, $x(1/2)_{s.m}$ = the monthly median of original data, $x(5/6)_{s.m}$ = the rainfall value demarking the upper sextile of original data, and the subscripts s, m, and y denote the station, month, and year, respectively. Values of R were calculated separately for original and filled data. For each calendar month, the proportion of stations for which R exceeded 4 was determined separately for original and filled data. For each calendar month, the maximum such proportion among all stations for original data was set as the threshold against which filled data were evaluated. If the proportion of months with R values in excess of 4 for filled data was greater than the threshold set for the month, all the filled data for that station-month were rejected. For example, Figure A5 shows the November plot of the proportion of filled and original months for which R exceeded 4. In this case, the proportion was never higher than 0.087 for the original data. The red lines on the right are for the filled data. The lines reaching above the 0.087 limit identify stations with problematic filled data for November. For those stations, the November filled data were rejected.

To analyze the left side of the distribution, a different procedure was used. In this case, the lowest sextile, set according to the distribution of original data for the station-month, was used to demark the lower extreme of the distribution. The expected relative frequency of monthly rainfall totals within that quantile is 0.167 (1/6). The actual relative frequency of rainfall values below the first sextile was calculated for each station and each month for the filled data, forming a set of relative frequencies for each calendar month. Using the mean and standard deviation of that set, thresholds of the mean plus or minus two standard deviations were used to identify filled data sets with too many or two few values in the lowest sextile. In Figure A6, a histogram is shown of relative frequencies of the lowest sextile for November filled data. In this case, stations with a relative frequency equal to zero or greater than 0.389 were rejected. A total of 1014 station months were removed based on these quality control criteria for the extremes of the frequency distributions.

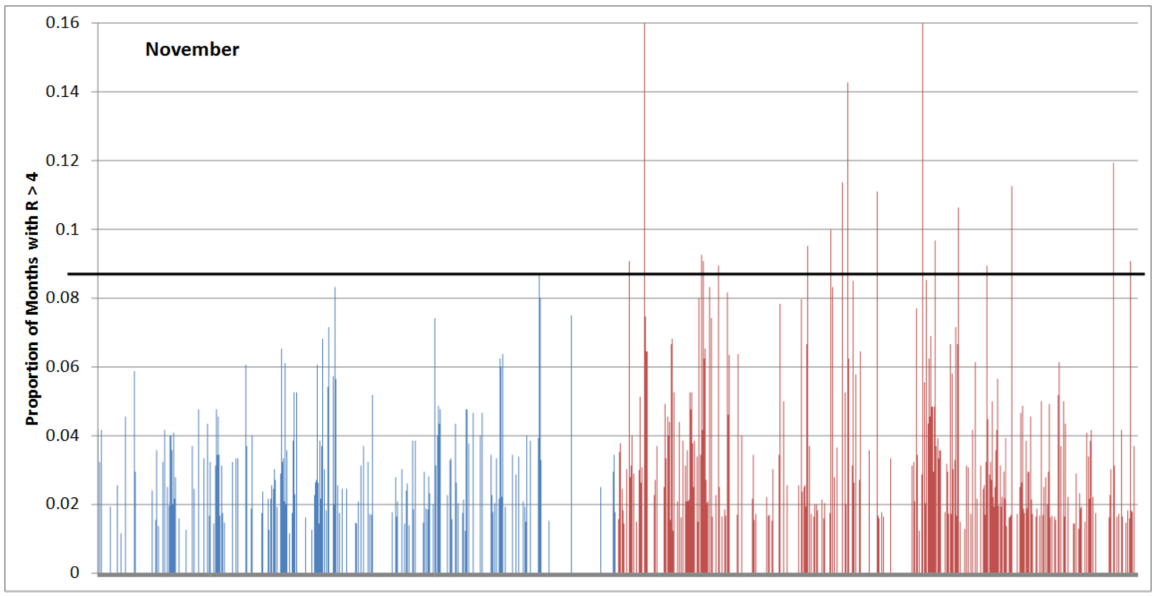

Figure A5. The proportion of months for which the value of R exceeded 4 for original data (blue) and filled data (red). The bold horizontal line positioned at a value of 0.087 on the y-axis demarks the maximum value found for the original data, and sets the upper limit for acceptable filled data.

Normal Ratio Refilling

Since the quality control steps removed numerous station months, this left many stations without a complete 30-year record for calculating the means. For some of these stations for which the Eischeid method failed, especially ones located near rainfall peak areas and where few other stations are found nearby, we made another attempt at gap-filling, using the simpler normal ratio method (Eq. l). This second round of gap filling allowed us to compute an additional 345 30-year monthly means.

Base Period Selection

Before calculating station monthly and annual mean rainfall, it was necessary to decide upon a common base period for averaging the records. In previous Hawai‘i rainfall analyses, a number of different averaging periods were used. The original Rainfall Atlas of Hawai‘i used the period 1916–1983 (68 years) for all islands except Moloka‘i, where 1931–1983 (53 years) was used. The length of the averaging period is the first question. Using a long period does a better job of averaging out the effects of slowly changing natural cycles, such as the Pacific Decadal Oscillation (PDO). On the other hand, because we are experiencing a long-term downward trend in rainfall, using a shorter averaging period may be better for characterizing the current and near future situation. The National Oceanic and Atmospheric

Administration (NOAA) uses a standard 30-year averaging period, with statistics updated at the end of each decade. Considering all these issues, and giving more weight to the recognition of the long-term trend in rainfall, we opted for a 30-year averaging period. We chose to use 1978–2007, which was the most recent 30-year period for which a high percentage of data for active stations were available as of the start of the project. We acknowledge that for most of this period, the PDO was in its positive phase, which is generally associated with lower rainfall.

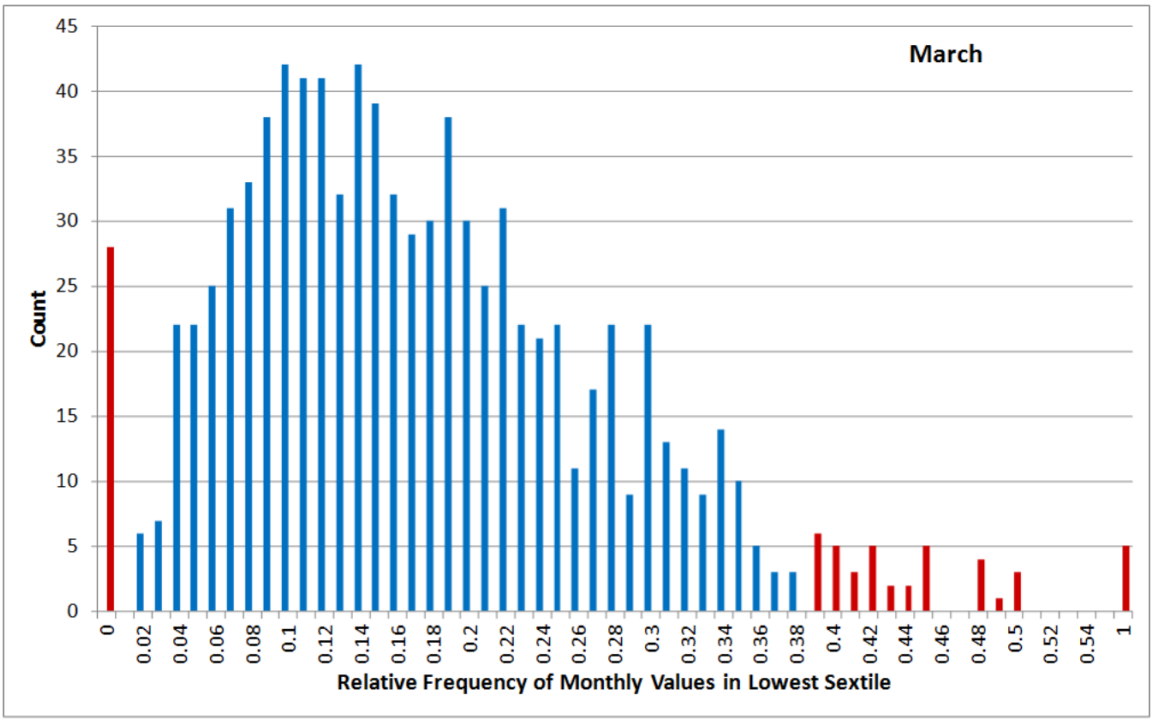

Figure A6. Histogram of the relative frequency of filled rainfall values below the lowest sextile, set based on original data, for all stations in March.

Improving Estimates of Station Coordinates

A great deal of work was done to correct and update the coordinates of the raingage stations. Multiple sources for the coordinates were obtained, which all provided different values for the same stations (including the state climatologist's master record of stations, which had the same problems as the other data received). It was unclear in most cases which sources to trust, and many techniques were used to acquire the best coordinates possible.

The first big discrepancy between sources was the datum. Most of the coordinates were given in the Old Hawaiian Datum (OHD), and needed to be converted to the North American Datum of 1983 (NAD83; Figure A7 shows the systematic shift caused by coordinates in the old datum) and later to the World Geodetic System

(WGS84). After making this correction, a significant number of stations were still being plotted in the ocean (Figure A8), making it was obvious that problems remained. Stations with coordinate errors were easy to identify when they plotted in the ocean. But, we had little confidence that coordinates were correct just because they plotted within the coastal boundaries. A few criteria were put in place to try and catch the errors on land. We used the published elevation of each station in comparison with the elevation of its supposed location, identified using a digital elevation model (DEM) to ferret out problems and resolve conflicts. When multiple sources were available for one station, the source whose DEM elevation was closest to the published elevation was chosen. If both stations were very close or very far from the real elevation, that station was examined more closely.

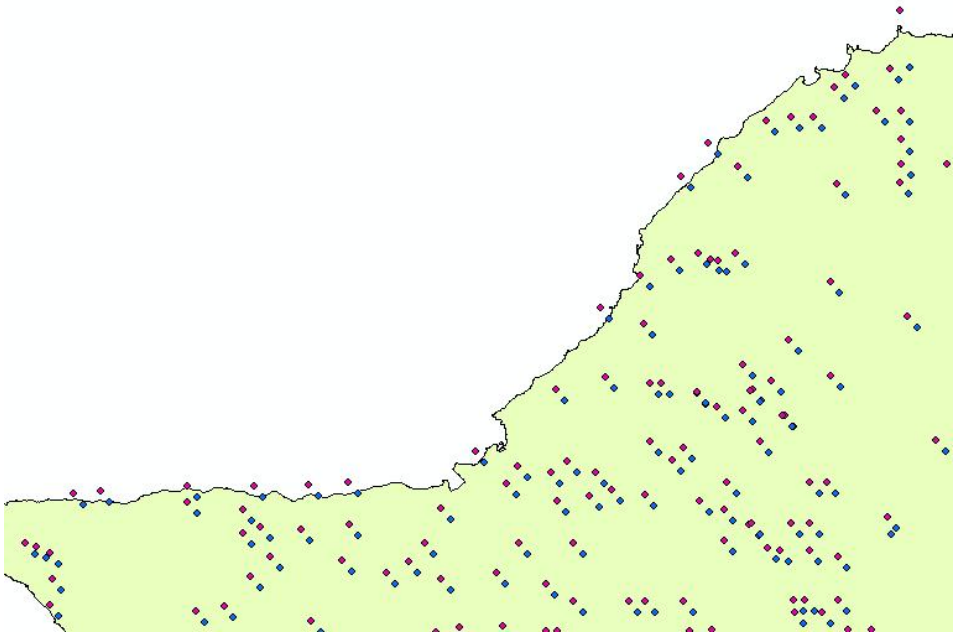

Figure A7. The stations plotted in pink are in the Old Hawaiian Datum, whereas the blue points are the same exact stations but converted to NAD83.

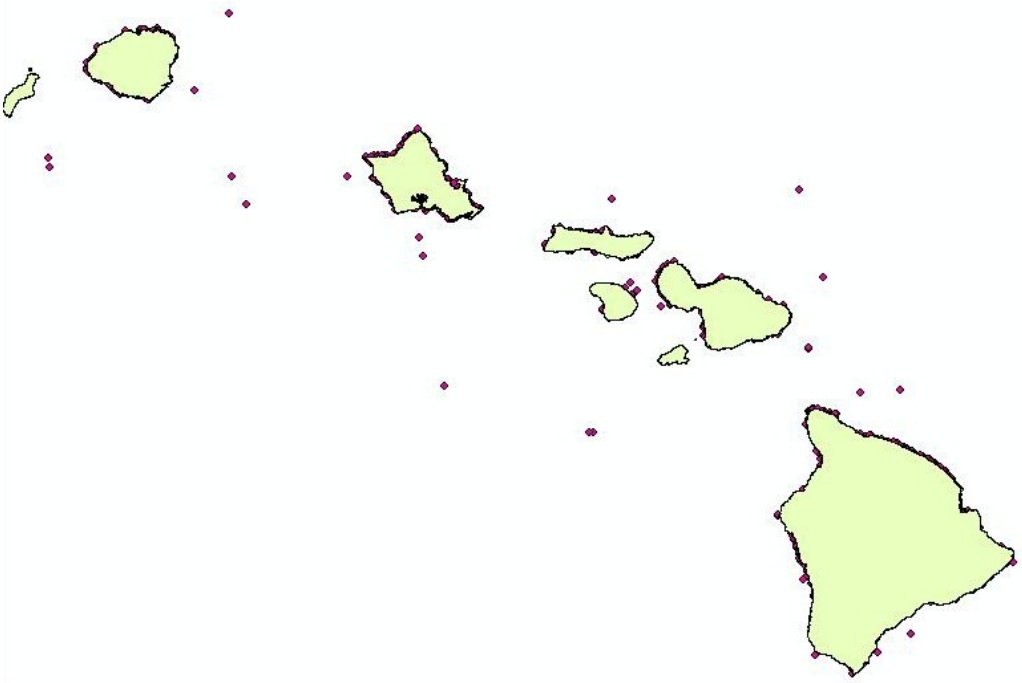

Figure A8. Most obvious location errors – stations plotted in the water.

In 1973, the State of Hawai‘i Department of Land and Natural Resources Division of Water and Land Development published a report entitled “Climatologic Stations in Hawaii”, Report R42. This report contained maps with all climate stations plotted, including raingage stations, and a table listing names, coordinates, and state key numbers of every station. Although this book contains some errors, it was the best resource for finding the original locations of the stations. In some cases, personal contacts were used to locate stations still in operation by certain agencies (current stations often have GPS-derived coordinates, which are more reliable). In the absence of other information, for stations with conflicting location information from multiple sources, priority was given to the small network station coordinates (because most of these were current networks with GPS coordinates), second priority to State data coordinates (which were scrutinized using the R42 report and elevation techniques), and last to NCDC coordinates (which were only precise to 0.001° latitude and longitude).

Uncertainty

The station means and maps of mean monthly and annual rainfall represent our best estimates for the 30-year base period 1978–2007. However, for many reasons, it is not possible to determine the exact value of mean rainfall for any location, even at the stations. In recognition of that, we provide estimates of the uncertainty in our estimates of station means and mapped means.

The uncertainty value that we provide can be interpreted as a plus-or-minus range around the estimated mean. While we cannot say exactly what the mean is, we are confident that it lies within that range. For example, mean annual rainfall for the US Geological Survey's Moanalua station (State Key Number 772.3) has an estimated mean annual rainfall of 3317 mm (130.6 inches) and an uncertainty of 128 mm (5.0 inches). That means the true mean annual rainfall for the base period is likely to be between 3189 and 3445 mm (125.6 and 135.6 inches). The uncertainty statistic we use is in the form of a standard deviation. If we assume the sample of possible estimated means has a normal ("bell-shaped") distribution, then the likelihood of the true value being within ±1 standard deviations from the mean is about 68%.

Many different things influence the level of uncertainty. In the case of the station means, we considered three sources of uncertainty. The first is the number of values used to calculate the 30-year mean. We included stations with up to three missing values within the 30-year base period. But, we realize that the more missing values we have the more uncertain the resulting mean is. For each station with less than 30 years of data, we calculated the added uncertainty of each missing value and multiplied it by the number of missing values. The second source of uncertainty is related to the gap-filling process. Wherever possible, we made estimates of monthly rainfall to fill gaps in the records of stations. This was used to fill gaps within the period of record, such as when a gage was malfunctioning, and to fill periods before and/or after the gage operated. As a result, the 1978–2007 mean for a give station could have anywhere from 0 to 30 estimated (as opposed to measured) values. Gap-filling is essential for producing means that pertain to a common base period, and allows us to use a much larger number of stations than we would otherwise. But, obviously, an estimated monthly rainfall total is more uncertain than a measured one. We used calculated estimated values at all stations for all months, even those with measurements. This was done to allow us to compare the estimates with measurements. This gave us a measure of the uncertainty of the estimates at each station. This value was then multiplied by the number of estimated values to get the uncertainty resulting from gap filling. The third source of error was related to the station locations. In compiling the data set used in this analysis, we found that many errors existed in the published locations. Poor precision, conflicting information about station coordinates, use of an obsolete map datum, typographical errors, and other problems led to many stations being out of place on our maps. Some were even well out in the ocean. We worked hard to eliminate these problems, but were still unsure about the locations of stations, especially ones that had been long discontinued. Imprecision in the station location amounts to an uncertainty in the rainfall. Consider that in some areas, the rainfall gradient is so steep that a station misplaced by only 1 km (0.6 miles) could misrepresent actual mean rainfall by 1500

mm (59 inches). Using our estimated uncertainty in the location of each station, we used the local rainfall gradient to convert that into the resulting uncertainty in rainfall. The uncertainties from these three sources were combined to give the total uncertainty in each station mean.

Uncertainty in mapped rainfall results from the combined uncertainty of the interpolated station values, derived using ordinary kriging, and the uncertainty in all of the predictor data used to produce the map. In general, interpolation uncertainty is low near stations and increases as the distance to the nearest station increases. In other words, uncertainty is greatest where there are no nearby stations. The spatial patterns of uncertainty in radar-estimated rainfall, the MM5-estimated rainfall, and rainfall taken from the PRISM analysis, were estimated by comparing the mapped values with station values. When merging the predictor maps to get the final estimate at each location, the uncertainties in the predictors were also combined to get a map of total uncertainty at each location.

Estimating Uncertainty of Station Mean Rainfall

Uncertainty Due to Gap-Filling. For all of the stations that required filling to make the record complete, the filled data overlapped where there also existed original data, which allowed for cross validation in the quality control stage. This overlap also allowed the standard error of the gap-filled data to be computed, by comparing the estimates with the original data. The standard error was calculated for every station-month, and used as one of the three sources for station uncertainty. That value was weighted by the number of gap-filled values within the 30-year base period. If a station's data for a given month from 1978-2007 was entirely original data records, the gap-filling standard error was zero.

Uncertainty Due to Small Sample. The second source of uncertainty considered was the uncertainty resulting from the use of fewer than 30 values to estimate a 30-year mean. When generating the means for the period of 1978-2007, station months were required to have at least 27 complete years in that period, otherwise no mean was calculated for that station month. The majority of the stations had complete records for most months thanks to the gap filling. However, for the stations with less than 30 years within the base period, the small uncertainty generated by this needed to be included. A gamma distribution was fitted to the data for each of the station months that had samples of less than 30. Based on the gamma distribution and using a random number generator, 1000 values were stochastically generated for each missing value, generating 1000 possible values for the true 30-year mean. The standard deviation of those means was used as the estimated small sample uncertainty.

Location Uncertainty. The last type of uncertainty that was taken into account was the uncertainty in the location of the stations due to low confidence in the stated location and/or poor precision in the recorded geographical coordinates. Very few of the station coordinates were taken with a GPS unit in the field. Most coordinates recorded for stations that have been out of operation for many years were based on estimated locations plotted on topographic maps. Many of the stations were verified manually with the available sources. For others we were able to verify locations only by comparing the recorded elevation with the elevation at the location of the recorded coordinates, using a digital elevation model (DEM). Depending on the level of quality control and the confidence in the coordinates, an uncertainty radius was assigned to each station (1-arc-second, 3-arc-seconds, 5-arc-seconds, subsequently converted to meters, or a more specific value in meters if known). The NCDC stations, which had geographical coordinates expressed in decimal degrees to the third decimal place were given an uncertainty radius of 0.001°. Using the 1986 Rainfall Atlas, the slope of the rainfall surface for each month was obtained for every station location (mm rainfall per m horizontal distance). The slope was multiplied by the uncertainty diameter in meters to get the range of uncertainty in rainfall due to the in location uncertainty for each station. Assuming a uniform distribution, the standard error associated with this uncertainty range was estimated. The location uncertainty has a greater effect in areas with a steep rainfall gradient. In areas with a low rainfall gradient (low slope), imprecise or uncertain coordinates do not have as large an impact on the estimated rainfall.

Total Uncertainty

The three sources of uncertainty were combined to get total uncertainty in the form of the total error variance using the following equation:

$$Total\ Error\ Variance = FillingError^2 + SmallSampleError^2 + LocationError^2 \quad (3)$$

The filling error and small sample error were already in standard deviation terms, so only the location error had to be converted. These variance values were used in the final maps to resolve disputes between nearby stations.

Estimating Rainfall from Vegetation in the Hawaiian Islands

Vegetation ecologists have long recognized the influence of climate on vegetation, with rainfall being particularly important (Holdridge, 1967). This recognition is evident in early descriptions of vegetation in the Hawaiian Islands (Hillebrand 1888, Rock 1913). Modern objective treatments relating climate data to vegetation include

that of Ripperton and Hosaka (1942), and a more recent climatic-vegetation concept developed by Gagné and Cuddihy (1990). Increasingly, the availability of spatially explicit climate data, such as rainfall patterns derived from Giambelluca et al. (1986), permitted a detailed characterization of climate in Hawai‘i (Giambelluca and Schroeder 1998), and the exploration of quantitative linkages between rainfall and vegetation patterns. Despite the importance of climate, several other factors, including topography, soil, and disturbance history, all interact to influence the species composition and structure of vegetation (Major, 1951; Gagné and Cuddihy, 1990). In Hawai‘i, this is further complicated by various human impacts ranging from cattle ranching to invasive plant species (Cuddihy and Stone, 1990). Nonetheless, the advent of Geographic Information Systems, and the availability of maps representing these confounding influences, makes it possible to disentangle these factors in order to isolate the influence of climate. By making clear quantitative associations between mean annual precipitation and vegetation based on locations where both are well known, it is therefore feasible to estimate precipitation from vegetation in areas where no precipitation data are available.

Two vegetation maps provide the best opportunity for relating vegetation to rainfall patterns. The first, by Jacobi (1989), classifies vegetation into 89 distinct associations for the upland areas of the Islands of Hawai‘i, Maui, Moloka‘i and Lāna‘i. Drawing from extensive fieldwork during the Hawai‘i Forest Bird Survey, these maps categorize vegetation according to dominant species, canopy closure, canopy height, subcanopy indicator species, and moisture. In this classification scheme, all vegetation units are assigned to the Dry, Mesic or Wet moisture classes, which correspond generally to the concept outlined in detail by Gagné and Cuddihy (1990). Vegetation units defined as Wet have a significant cover of tree ferns and other fern species, and support prominent epiphyte communities (Jacobi, 1990). Those units defined as Mesic have a lower abundance of tree ferns and epiphytes (although these may occur), yet nonetheless lack a strong seasonality (i.e., grasses do not die back on a yearly basis, and the understory has ferns and other species that remain green in all months). Units defined as Dry exhibit very low cover of ferns, high grass or even bare rock/soil cover, and a strong seasonality (i.e., grasses die back in dry months). Figure A9 shows vegetation units according to Jacobi (1989) grouped according to moisture type. The moisture concept in this classification reflects not only aspects of climate, but additional influences on vegetation such as substrate age and degree of human disturbance. For example, areas with a young lava substrate are classified as being Mesic even if they fall within a region of extremely wet climate as seen on the east side of the Island of Hawai‘i (Figure A9). Similarly, in areas with a Wet climate where vegetation has been disturbed by clearing and cattle grazing and where invasive grasses have become dominant, vegetation is classified

as Mesic or even Dry, as seen on the west side of the Island of Hawai‘i. Therefore, only those areas representing relatively undisturbed native vegetation in areas with well-developed soil are useful in relating vegetation patterns to rainfall.

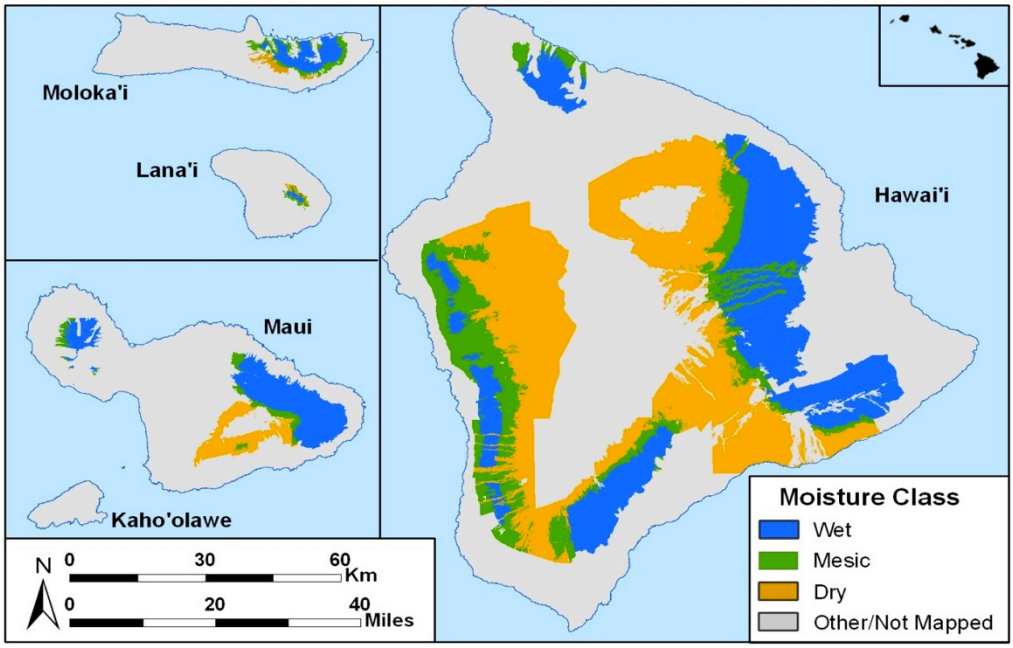

Figure A9. Moisture zone map by Jacobi (1989). Vegetation classes were consolidated to show moisture classification.

A map by Gon et al. (1998) covers the entire state (Figure A10), albeit at a somewhat lower spatial resolution than Jacobi's (1989) map. It represents the same basic moisture concept as Jacobi (1989) and Gagné and Cuddihy (1990), although it does not distinguish areas undergoing primary succession on young lava, and classifies areas that have been disturbed by cattle ranching and other human activity as being non-native vegetation. Similarly, it is most useful in areas where complications associated with human disturbance and young substrates are minimal. The boundaries between the moisture classes represented on these maps are expected to occur consistently at some rainfall threshold. Gagné and Cuddihy (1990) defined Dry as areas receiving less than 1200 mm mean annual precipitation (MAP), Mesic as areas receiving between 1200 and 2500 mm MAP, and Wet as areas receiving more than 2500 mm MAP. Price et al. (2007) found that moisture class boundaries did not fit precisely with these values, however, due to likely differences in potential evapotranspiration (PET), which varies with elevation (Juvik et al., 1978; Bean et al., 1994; Juvik and Tango 2003).

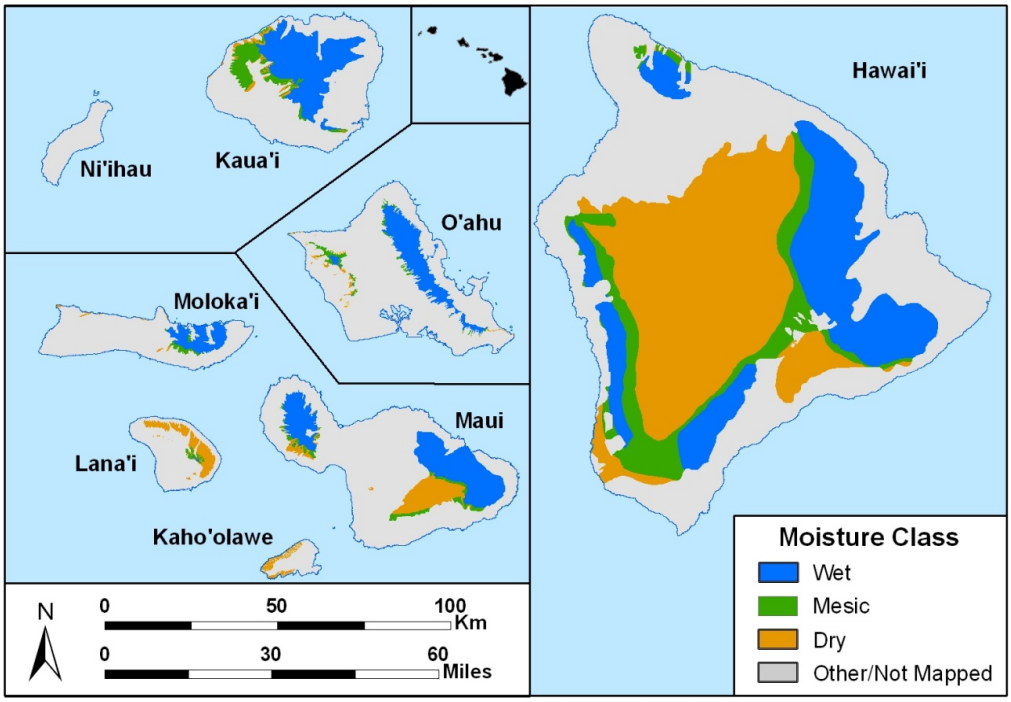

Figure A10. Moisture zone map by Gon et al. (1998). Vegetation classes were consolidated to show moisture classification.

Methods for Using Vegetation to Estimate Rainfall

A series of calibration locations was selected to represent boundaries of major climatic vegetation types where a reliable estimate of MAP is available. Several criteria ensured that both the vegetation and the estimated MAP were accurately represented. The Geographic Information System program ArcGIS (ESRI, 2009) permitted a precise spatial rendering of various features and a coordinated selection process. First, locations were chosen at either the Dry-Mesic boundary or the Mesic-Wet boundary as broadly defined by the broadly accepted concepts of these moisture classes. Where possible, Jacobi's (1989) map was used, because of its higher spatial resolution and greater precision; however, because the Jacobi map covers only some of the islands, the map by Gon et al. (1998) was used otherwise. In a few cases, the two maps disagreed on the location of a vegetation boundary, and so it was necessary either to choose the map that was considered to be more precise (usually Jacobi) or to compromise under the assumption that each erred slightly in opposite directions. In a small number of cases, locations based on field observations (J.P. Price, unpublished data) were used to extend the number of observations. To ensure vegetation was not overly influenced by young substrate age (which tends to make vegetation appear "drier" than the actual climate), we used the criteria outlined by Price et al. (2007) by employing geologic maps by Wolfe and Morris (1996) and Sherrod et al. (2006) to exclude areas where substrate

age was likely young enough to influence vegetation strongly. In addition topographic maps ensured that calibration locations were not on cliff faces (which tend to have more sparse vegetation than the climate would indicate) or gulch bottoms (where hydrology makes more moisture available than that provided by precipitation). Several maps including Jacobi (1989) and the HIGAP landcover map (Gon, 2006) were used to exclude areas considered to be too heavily altered by cattle ranching and other human activity. Finally, calibration locations were located within 3 km of a climate station used in the present rainfall atlas. While few stations fell precisely at any vegetation boundary, a representative number were relatively close. Due to the sharpness of precipitation gradients, rather than use the MAP values of the stations themselves, we used MAP at a given location on a vegetation boundary from a preliminary interpolation of station data. A total of 17 locations met these criteria for the Dry-Mesic boundary (Table A2), and 30 locations met these criteria for the Mesic-Wet boundary (Table A3). These locations were fairly well distributed across the State and represent a range of elevations (Figure A11).

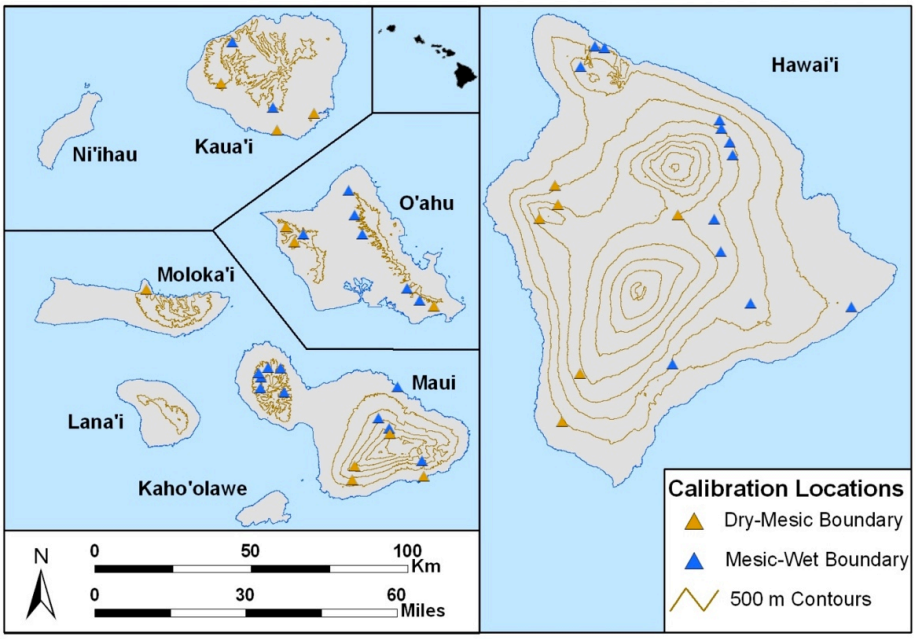

Figure A11. Sites used to relate rainfall to different vegetation boundaries.

Gagné and Cuddihy (1990) estimated the Dry-Mesic boundary to receive 1200 mm MAP) and the Mesic-Wet boundary to receive 2500 mm MAP. While these may approximate average values for those boundaries, based on Price et al. (2007), we expect the MAP thresholds to be slightly lower at middle elevations, where PET is lower (Juvik et al., 1978; Bean et al., 1994; Juvik and Tango, 2003) and therefore a lesser amount of rainfall is needed to maintain a given moisture balance. To test

Table A2: Calibration sites at Dry-Mesic Boundary. Calibration sites are identified by the nearest station. Estimates of mean annual precipitation come from preliminary interpolation of rainfall from established stations. Maps used to determine the location of the Dry-Mesic boundary include: 1) Jacobi (1989), 2) Gon et al. (1998), and 3) incidental observations (see main text for descriptions).

Nearest Station	SKN	Elevation (m)	MAP (mm)	Map used
Puu Waawaa	94.1	1000	654	1
Manuka	2	450	879	2
Auwahi	252	800	578	3
Haleakala Ranger	338	2200	1273	1
Kalawao	563.1	100	1145	3
Wailupe Res 170	723.2	300	1429	2
Makaha	842.1	600	1402	2
Makua Ridge	842.9	500	1203	2
Kitano	1037.1	600	959	2
Malumalu	1017	0	1400	3
Kukuiula	935	0	1212	3
Honuaula	71	1900	954	1
Halepiula Shed	70.1	1500	665	1
Castle	2.26	1850	1057	1
Kalaeeha	80	2000	899	1
Kaupo Store	257.4	50	1365	3
Polipoli Spring	267.2	1800	820	2

Table A3: Calibration sites at Mesic-Wet Boundary. Calibration sites are identified by the nearest station. Estimates of mean annual precipitation come from preliminary interpolation of rainfall from established stations. Maps used to determine the location of the Dry-Mesic boundary include: 1) Jacobi (1989), 2) Gon et al. (1998), and 3) incidental observations (see main text for descriptions).

Nearest Station	SKN	Elevation (m)	MAP (mm)	Map used
Awini	182.1	500	3100	1
Kaukini	184.1	500	3300	1
Maulua	126	1600	2867	1
Nauhi	128	1600	3188	1
Hawaii Nat	54	1200	2500	1
Honomanu Gulch	341	1500	2960	1
Wood Valley	35.6	800	2212	1
Kahoma Intake	374	1000	2432	1,2
Honokowai	476	800	2974	1
Kulani School	78	1800	2241	1
Manoa Tunnel 2	716	400	3000	2
Iao Needle	387.2	300	2820	3
Saddle House	82.1	1650	2374	1
Ukulele	333	1300	2605	2
Kokee	1076	1200	1651	2
Alexander Res	983	600	2484	2
Kawai iki	8880	400	2525	2
Last Tunnel Out	878	400	2962	2
Honokohau	480	700	2986	1
Manoa Tunnel 2	716	400	2918	2
Kailua	446	0	2858	3
Kamaile	67	200	2731	3
Haelaau	477	700	2528	1,2
Kahakuloa	482.4	700	2426	1
Panileihulu	259.2	1300	3138	1
Old Pali Road	783.3	500	2736	2
Mount Ka‘ala	844	1000	1838	2
Kehena	181.2	1200	2103	1
Keanakolu	124	1450	2430	1
Pupukea 1	898	300	2114	2

this, second order polynomial regression analysis was performed, using elevation of a calibration location as the independent variable and the MAP as the dependent variable. If lower PET has an influence on the vegetation boundary, the rainfall at a given boundary should be less at middle elevations than at higher or lower elevations, where more rainfall is needed to maintain a given moisture balance. The resulting equations may then be used to estimate the MAP at any location along a given boundary.

To select locations where rainfall estimates are needed a similar set of criteria must be met. The boundary should be clearly mapped, should be on relatively neutral topography (e.g., not on cliffs or gulch bottoms), should be in areas with good soil development (e.g., not young lava flows), and should be relatively free of severe habitat degradation. Among areas that met these criteria, areas were selected where the raingage network is sparse making it likely that rainfall interpolation would be poor. Areas such as East Moloka‘i and the Ka‘ū district of the Island of Hawai‘i had generally few stations present and so supplemental stations were needed for accurate assessment of rainfall patterns. In other cases, even where several stations are nearby, these do not properly reflect gradients in rainfall. For example, on West O‘ahu, there are stations on either side of the southern Waianae Mountains, yet none near the summit crest, potentially leading to an underestimation of rainfall in between stations. In other cases locations with extremely sharp gradients associated with steep topography may benefit from strategically placed estimation locations. Once an estimation location was established, the elevation can be used to estimate the approximate MAP of the boundary associated with that site.

Results of Using Vegetation to Estimate Rainfall

Calibration locations for the Dry-Mesic boundary had a mean MAP of 1052.6 +/- 279.3 mm. A second order polynomial regression indicates statistically significant concave relationship, whereby MAP of this boundary is approximately 1400 mm near sea level, dropping to below 800 mm at about 1200 m elevation, then increasing past 1000 mm above 2000 m elevation (Figure A12).

Calibration locations for the Mesic-Wet boundary had a mean MAP of 2633.4 +/- 406.5 mm. A second order polynomial regression indicates statistically insignificant concave relationship, whereby MAP of this boundary is approximately 3000 mm near sea level, dropping to about 2500 mm at about 1200 m elevation, then increasing with elevation above that (Figure A13). This pattern, while not significant, is likely a better estimate than simply using the average of 2633.4 mm MAP for all locations along the Mesic-Wet Boundary.

Estimates were made at eight locations along the Dry-Mesic boundary (Table A4; Figure A14) and at twenty-two locations along the Mesic-Wet boundary (Table A5; Figure A14). Some areas (especially East Molokai) have a large concentration of estimate locations relative to the number of actual climate stations, and therefore much of the ultimate interpolated MAP for the area will rely on these.

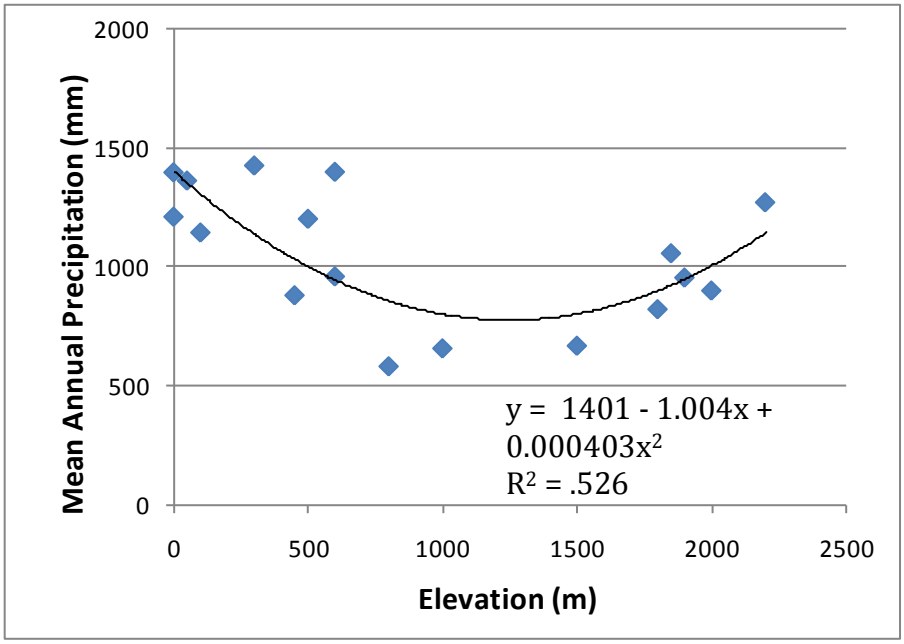

Figure A12. Elevation vs. Mean Annual Precipitation at the Dry-Mesic boundary. Estimates of mean annual precipitation come from preliminary interpolation of rainfall from established stations.

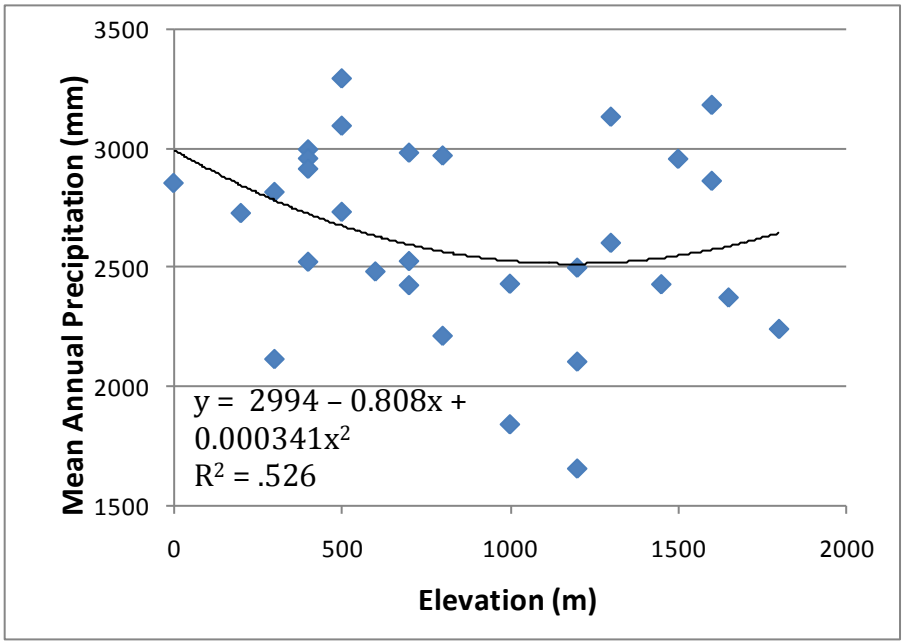

Figure A13. Elevation vs. Mean Annual Precipitation at the Mesic-Wet boundary. Estimates of mean annual precipitation come from preliminary interpolation of rainfall from established stations.

Table A4: Estimation sites at the Dry-Mesic Boundary. Estimation sites are identified by a general description of the location. Estimates of mean annual precipitation come from application of regression equation given in Figure A12 based on elevation of each site. Maps used to determine the location of the Dry-Mesic boundary include: (1) Jacobi (1989), (2) Gon et al. (1998), and (3) incidental observations (see main text for descriptions).

Location	Island	Elevation (m)	MAP (mm)	Map used
Honuliuli	O‘ahu	450	1031	2
Palehua	O‘ahu	600	944	2
Kamalo	Moloka‘i	600	944	1,3
Kawela	Moloka‘i	800	856	3
Holua	Maui	2100	1070	1,3
Paliku	Maui	2000	1005	1,3
Kahikinui	Maui	2000	1005	1
Great Crack	Hawai‘i	450	1031	1,3

Vegetation-based Rainfall Estimates: Discussion

The mean MAP value for the Dry-Mesic boundary (1052.6) was somewhat below the value of 1200 mm given by Gagné and Cuddihy (1990). This is best attributed to the fact that most areas occurring at this boundary are at low elevation: apart from Maui and the Island of Hawai‘i, the entire Dry-Mesic boundary lies below 800 m elevation. Considering that lower elevations had somewhat higher MAP values along the boundary in the regression model, Gagné and Cuddihy's (1990) assertion of a 1200 mm threshold is probably consistent with most observations. Nonetheless Mesic conditions can occur at areas with as little as 800 mm MAP at middle elevations where cloud cover is frequent, humidity is high, and solar radiation is low, all of which depress PET. This underscores the long-held view that PET strongly influences overall moisture balance (Thornthwaite, 1948; Holdridge, 1967).

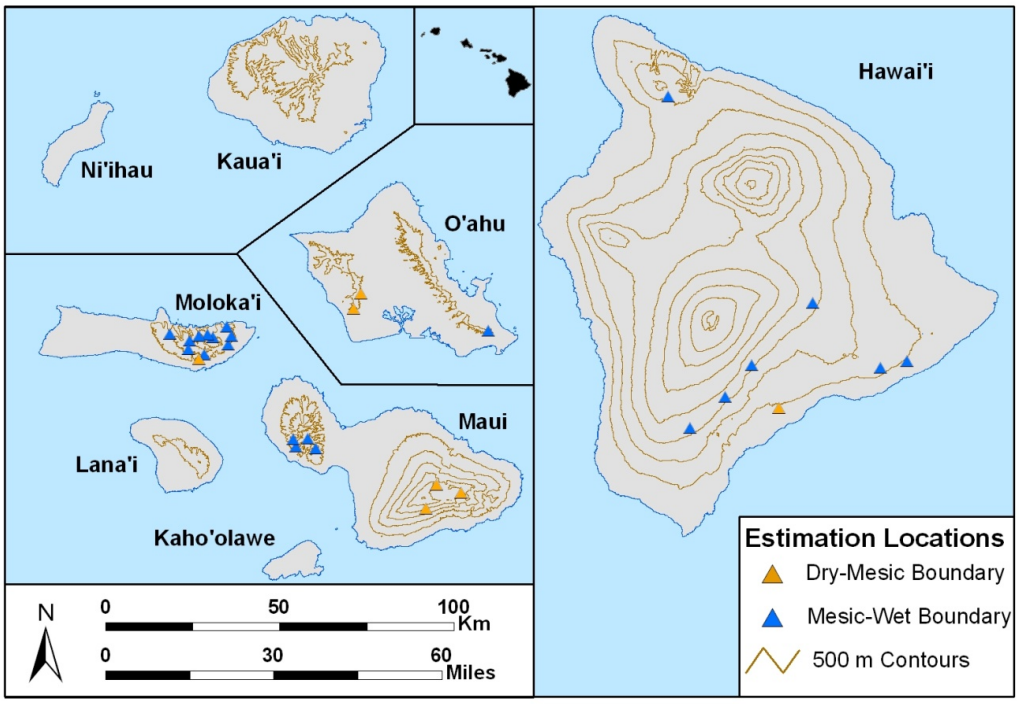

Figure A14. Estimation Locations. Sites for which rainfall was estimated based on the vegetation-rainfall relationship.

The mean MAP value for the Mesic-Wet boundary (2633.4) is somewhat higher than that given by Gagné and Cuddihy (1990), although in this case the standard deviation was somewhat high. This was reflected in the weakness of the regression: despite the fact that the pattern of the regression equation was remarkably comparable to that for the Dry-Mesic boundary (with a mid-elevation dip), over one third of the sites exhibited a greater than 400 mm difference between the predicted and actual values. This may stem from several possible factors. First, there may be other aspects of climate that are underappreciated, such as the ability of fog to

enhance precipitation in highly localized and idiosyncratic ways. For example Juvik et al. (2010) found fog inputs significantly above the measured MAP on ridge tops on the island of Lāna‘i with an introduced species of tree that was able to enhance fog drip due to its structural. This suggests that fog may add significantly to the available moisture at some sites independently of rainfall. Wind certainly has spatial variation, and may either enhance fog drip or increase PET, making its relationship to overall moisture uncertain. It may also be that other factors in these remote areas (soil, topography, etc.) exert a stronger influence than was appreciated, and therefore the relative influence of rainfall on vegetation may be difficult to resolve. These confounding factors may impose considerable uncertainty on where a given boundary may be mapped. Considering the steepness of most precipitation gradients, however, it should not be surprising that a given boundary deviates from the expected value by several hundred mm. Considering that in many areas travelling as little as one km one can expect a drastic change in MAP, a boundary that has a spatial error of a few hundred meters is likely to translate into a MAP estimate very different that what may actually be recorded.

A major caveat associated with the technique developed here is the disparity between the timing of the base period and the relevant period of time reflected in the vegetation. Most vegetation observation in the field and aerial photos used in vegetation mapping were gathered in the 1970s and 1980s well before the base period for the present assessment. Using vegetation as perceived during one period of time to estimate precipitation during another period of time runs the obvious risk of not detecting decadal scale changes in MAP. This is particularly relevant since shifts in patterns of temperature (Giambelluca et al., 2008) and precipitation (Chu and Chen, 2005) are now becoming evident. Even if it were possible to re-evaluate vegetation structure and composition under changing climate, it may be that major components of vegetation (especially long-lived trees) reflect longer-term climatic averages and may not respond to any recent shifts in climatic averages.

Despite the level of uncertainty associated with mapping vegetation, isolating areas with expected to have the clearest climate signal, and relating this to reliable climate data, this method represents a significant improvement upon reliance on incomplete climate records. In remote locations, such as East Moloka‘i and the Ka‘ū district of the Island of Hawai‘i, prior to the addition of vegetation-based estimates, rainfall estimates were inaccurate over large areas. The former case includes several entire watersheds that receive significantly more precipitation than that estimated purely from existing climate stations. This exercise also helps identify important gaps in collection of climate data, such that strategic positioning of climate stations may improve future estimates.

Table A5: Estimation sites at the Mesic-Wet Boundary. Estimation sites are identified by a general description of the location. Estimates of mean annual precipitation come from application of regression equation given in Figure A13 based on elevation of each site. Maps used to determine the location of the Dry-Mesic boundary include: (1) Jacobi (1989), (2) Gon (2006), and (3) incidental observations (see main text for descriptions).

Location	Island	Elevation (m)	MAP (mm)	Map used
Oahu-Kuliouou	O‘ahu	700	2595	2
Mo-Waileia	Moloka‘i	900	2543	1
Mo-Pelekunu-W	Moloka‘i	700	2595	1
Mo-Pelekunu-E	Moloka‘i	300	2782	1
Mo-Kamakou	Moloka‘i	1200	2515	1
Mo-Kaluaaha	Moloka‘i	800	2566	1
Mo-Wailau-W	Moloka‘i	350	2753	1
Mo-Wailau-E	Moloka‘i	100	2917	1
Mo-Papalaua	Moloka‘i	600	2632	1
Mo-Halawa-	Moloka‘i	600	2632	1
Mo-Puniohua	Moloka‘i	600	2632	1
Ma-Helu	Maui	1200	2515	1
Ma-Lihau	Maui	1100	2518	1
Ma-Hanaula	Maui	1100	2518	1
Ma-Iao-Back	Maui	700	2595	3
Ha-Waimea-	Hawai‘i	1200	2515	2
Ha-Kulani	Hawai‘i	1600	2574	1
Ha-Kalapana1	Hawai‘i	700	2595	1
Ha-Kalapana2	Hawai‘i	400	2725	1
Ha-Kapapala	Hawai‘i	1600	2574	1
Ha-Kau-Central	Hawai‘i	1650	2589	1
Ha-Kau-West	Hawai‘i	1650	2589	1

Rainfall Maps Derived from Radar Observations

One of the predictor datasets used in the 2011 Rainfall Atlas of Hawai‘i was the set of rainfall maps derived from radar observations, specifically, data from NEXRAD (Next-Generation Radar), Weather Surveillance Radar 88 Doppler, WSR-88D Portion.

Radar Rainfall Estimation

Radar rainfall estimation is based on a relationship between the radar reflectivity (Z) and the precipitation rate (the Z-R relationship). The reflectivity measured by the radar is related to the dielectric constant and the number and size distribution of the raindrops. The rainfall rate is determined by the drop size and fall velocity distributions. Combining relationships for reflectivity and rainfall rate yields a Z-R relationship of the form:

$$Z = aR^b \quad (4)$$

For WSR-88D, the default Z-R relationship is $Z=300\ R^{1.4}$, which is a compromise between the relationships for stratiform and convective systems.

Four NEXRAD stations are operated in Hawai‘i, three of which were tested for use in the Rainfall Atlas. Table A6 gives the characteristics of the four Hawai‘i NEXRAD stations. Figure A15 shows the coverage of each station.

Table A6. NEXRAD stations in Hawai‘i

Station	Code	Latitude	Longitude	Elevation (m)
South Kaua‘i	PHKI	21°53’39.012"N	159°33’07.992"W	55
Moloka‘i	PHMO	21°07’58.008"N	157°10’48.000"W	415
Kamuela	PHKM	20°07’32.016"N	155°46’40.008"W	1162
South Shore	PHWA	19°05’42.000"N	155°34’08.004"W	418

We used the method of Horn and Kunz (2008) to convert radially arranged NEXRAD data into a rectangular grid pattern using the official National Climatic Data Center (NCDC) NEXRAD Exporter, version 1.9.11 (upgraded version available at NCDC Weather and Climate Toolkit, http://www.ncdc.noaa.gov/oa/radar/jnx/index.php). The NEXRAD exporter uses a ~ 0.005° resolution latitude-longitude grid based on the World Geodetic System spheroid (WGS84) to georeference the cells.

The National Weather Service office at Honolulu provided the WSR-88D 3-hr accumulated rainfall for 0300, 0600, 0900, 1200, 1500, 1800, 2100 and 0000 UTC every day for the 60-month period 2004-2008. Missing data were filled using temporal interpolation. The monthly rainfall accumulation map was compiled by summing the eight 3-hr accumulated rainfall totals every day for each for each spatial grid within the range of each radar site.

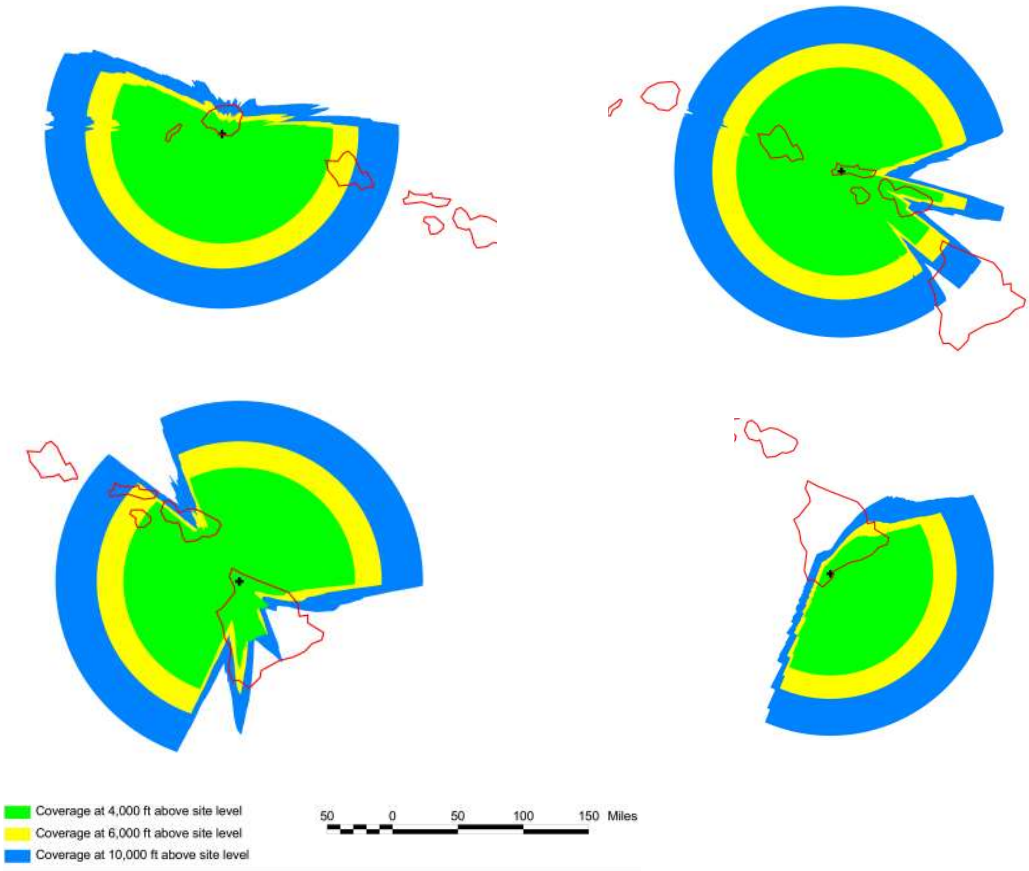

Figure A15. NOAA radar coverage maps for South Kaua‘i (upper left), Moloka‘i (upper right), Kamuela (lower left), and South Shore (lower right) NEXRAD stations (http://www.ncdc.noaa.gov/nexradinv/).

To improve data quality for radar-based rainfall mapping, it was necessary to identify and remove ground clutter. According to the National Oceanic and Atmospheric Administration (NOAA), the usable data coverage area for each radar site in Hawai‘i is depicted in the maps shown in Figure A15.

Ground Clutter, Terrain Blockage, and Radar Beam Height Effects

Radar observations typically contain spurious returns called clutter, which can be divided into two classes: surface clutter and volume clutter (Bassem and Mahafza, 2000). To develop useful radar rainfall results, it is necessary to identify and remove clutter.

Understanding how the radar beams are blocked by surrounding obstacles is important in the proper interpretation of reflectivity data. Kucera et al. (2004) developed a geographic information systems (GIS)-based method for estimating terrain effects on radar. We applied their radar beam propagation model,

incorporating digital elevation model (DEM) data, to calculate the effects of range-dependent power loss and terrain on the radar signal of each Hawai‘i NEXRAD site.

The height of a radar beam increases with increasing range (Figure A15). The height of the radar beam over a particular point, which is also determined by the height of the radar site, affects data quality. Precipitation from the shallow trade-wind clouds contributes a large amount of the rainfall to the annual accumulation in many areas. Trade-wind cumulus clouds have an average cloud base height of 600-800 m and the depth of about 1,000 m (LeMone and Pennell, 1976; Stevens, 2005). Cloud tops are generally found below the trade-wind inversion, at around 2,200 m.

The height of the center of the radar beam can be calculated as a function of range using the method of Doviak and Zrnić (1984) as:

$$h = [r^2 + (k_e a)^2 + 2rk_e a \sin\theta_e]^{1/2} - k_e a, \quad (5)$$

where h is the height of the radar beam, r is the slant range from the radar (r = x/cos($\theta_e - \theta_{1/2beam}$), x is the horizontal projection of r, k_e is 4/3, a is the earth's radius, and θ_e is the elevation angle. For the purpose of determining the spatial radar coverage, it is better to use the height of the bottom of the radar beam, as estimated by Maddox et al. (2002):

$$h = [r^2 + (k_e a)^2 + 2rk_e a \sin(\theta_e - \theta_{1/2beam})]^{1/2} - k_e a, \quad (6)$$

where θ_e is the elevation angle of the center of the radar beams, $\theta_{1/2beam}$ is the angle of a half of the radar beam width, r is the slant range from the radar.

We computed the height of the bottom of the radar beam for the South Kaua‘i, Moloka‘i, and South Shore radar sites, with θ_e, equal to 0.5° and 1.45°, the lowest two elevation angles of the center of the radar beam, and $\theta_{1/2beam}$, equal to 0.95°/2. The radar coverage maps calculated using the lowest elevation angle (θ_e = 0.5°) are comparable to the maps provided by NOAA (Figure A15).

Assessment of Each Radar Site

By taking into consideration ground clutter effects, terrain blocking, and beam height, we evaluated each radar site to determine areas where useful rainfall estimates might be obtained, as described below.

South Kaua‘i site. We found that the South Kaua‘i radar rainfall estimates are limited to southeastern Kaua‘i. This radar tends to receive weak echoes and, therefore, to underestimate rainfall at greater distances from the radar site (e.g., northern Kaua‘i and O‘ahu). Also, if the elevation angle of the radar beam is set to 0.5°, the radar

beam is blocked by the terrain along the entire southern coast of Kaua‘i. The second tilt angle (1.45°) may be used for southeastern Kaua‘i. The radar beam blockage by the terrain over the southwest Kaua‘i coast causes power loss and underestimation of derived rainfall behind terrain obstructions.

It is clear that the South Kaua‘i radar underestimates the 5-year mean annual rainfall over the southern Oahu (Figure A16, upper left) as compared with the Moloka‘i radar (Figure A17, upper right). This may be due to the Kaua‘i radar beam spreading with greater distance and to the higher radar beam height over southern O‘ahu (>8000ft ~ 2.4 km in), where it measures only high-altitude precipitation above the trade-wind inversion height (TWI~ 2 km). For accurate rainfall estimation, it is better to use radar beams with relatively low height that measure precipitation below the cloud base or lower portion of clouds. Because of this, we decided to use only the Moloka‘i radar for O‘ahu rainfall estimation.

Moloka‘i site. The radar-derived 5-year mean annual rainfall (mm) from the Moloka‘i site (Figure A16, upper right) suggests that this radar may provide reasonable estimates of the rainfall patterns over O‘ahu and part of Moloka‘i, Lāna‘i and parts of Maui. Some abnormal high rainfall values (Figure A17, upper right) correspond well with points with (0.5°) beam blockage (Figure A15, upper right). Behind terrain obstructions, the power of radar beam diminishes significantly. Thus, we identified these areas as part of the ground clutter. The NCDC coverage map (Figure A15, upper right) corresponds well with our analysis in this case.

Kamuela site. The Kamuela radar is located at a much higher elevation (1162 m) than other three radar sites in Hawai‘i (55, 415, and 418 m, respectively; see Table A6). From its vantage point, this site can detect precipitation over northern and western Hawai‘i Island, most of Maui, and southern Lāna‘i (Figure A15, lower left) at levels varying from 1,200 to 2,400 m above sea level. Because the precipitation from low-level trade-wind clouds is excluded, estimates from the Kamuela site were judged to be inadequate for use in this study.

South Shore site. The South Shore site was established mainly to monitor storm rainfall approaching from the ocean. The radar-derived 5-year mean annual rainfall (mm) derived from this radar (Figure A16, bottom) suggests that it is not very effective for observing the rainfall pattern over Hawai‘i Island, due to ground clutter and terrain blocking. The rainfall over the southeastern Big Island may be derived from the measurement taken at the second tilt angle (1.45°), whereas to the south, the 0.5° beam angle is appropriate. The effects of sea clutter, because of ocean waves, are evident over the ocean to the southeast of the site.

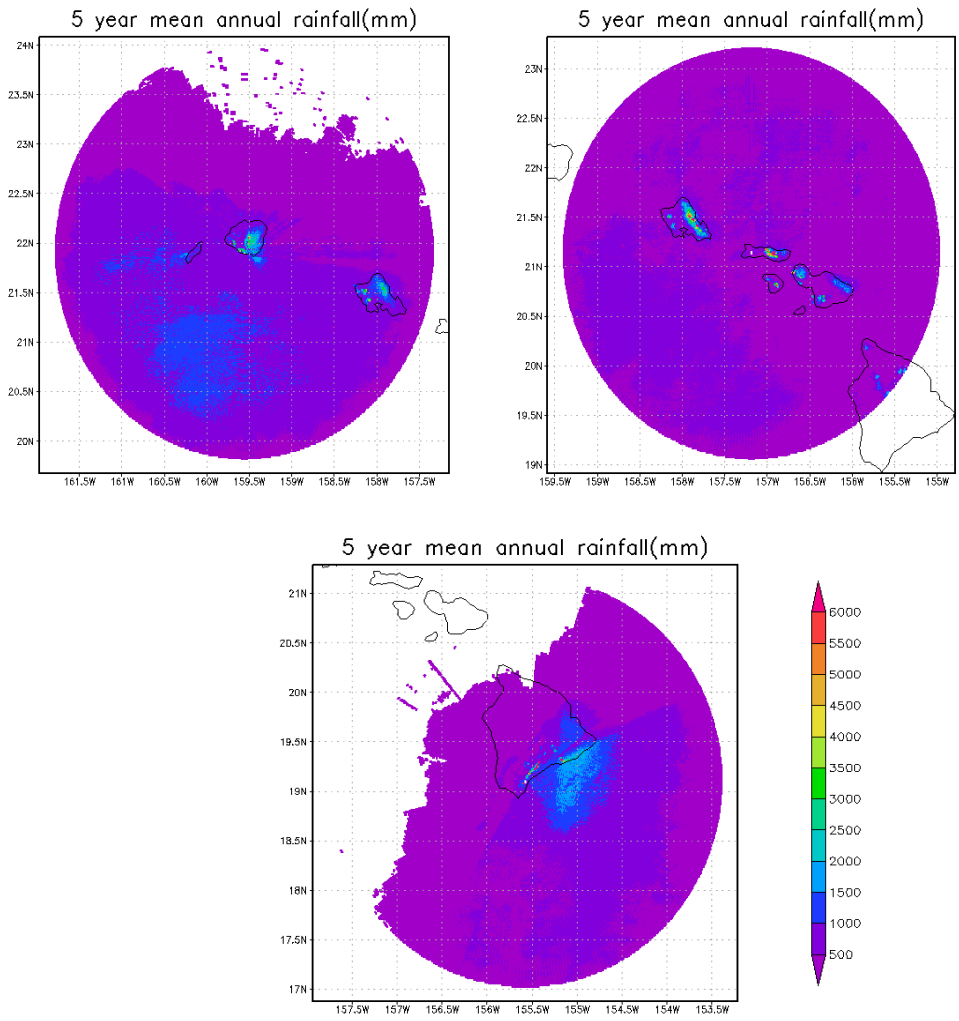

Figure A16. Radar derived 5-year mean annual rainfall (mm) for the South Kaua‘i (upper left), Moloka‘i (upper right), and South Shore (lower) NEXRAD stations.

Evaluation of Radar Rainfall Estimates

Using the Moloka‘i radar, which covers almost all of O‘ahu , we compiled the 2-month rainfall accumulation for July-August 2005 and compared it with ground-observed rainfall data (Nguyen, 2010). In general, the pattern and amount of rainfall estimated by the radar is similar to that derived from raingages (Figure A17). We further evaluated the radar rainfall estimates in the process of developing rainfall maps (described later in the section “Mapping Rainfall by Fusing Different Data Sources”).

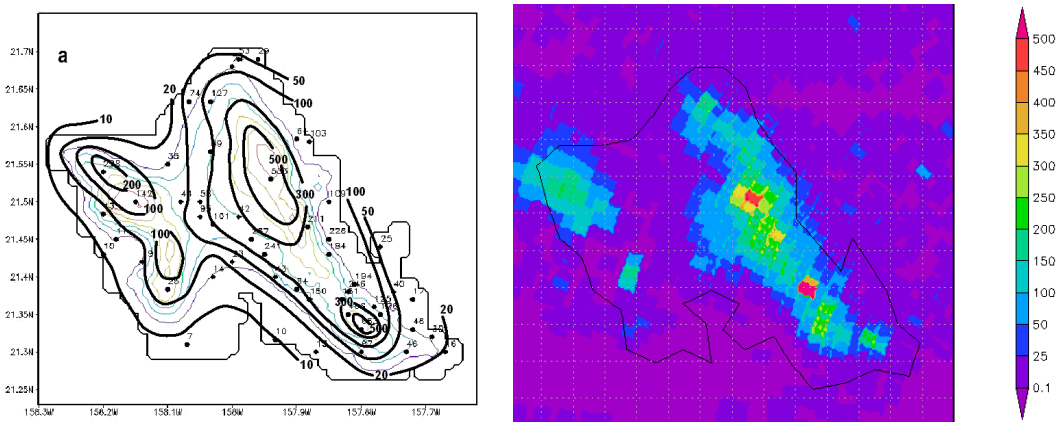

Figure A17. Total rainfall accumulation (mm) for surface observation (left; Nguyen 2010) and radar derived rainfall (right).

Radar Data Preprocessing

The radar rainfall maps appear to have noise in circular patterns, related to the range-based scanning pattern of radar (Figure A18, left). It is difficult to remove these circular strips of noise using a spatial filter since it may require a very large neighborhood window, which will smooth the local rainfall details. Given that the noise appears to have regular circular pattern and associated with a certain frequency, we can remove it in the frequency domain. This method works as follows: we first used Fourier transform to convert the image into the frequency domain and then identified the signals corresponding to the strips and removed them. In the end, the spatial images were reconstructed from the frequency domain (Figure A18, right).

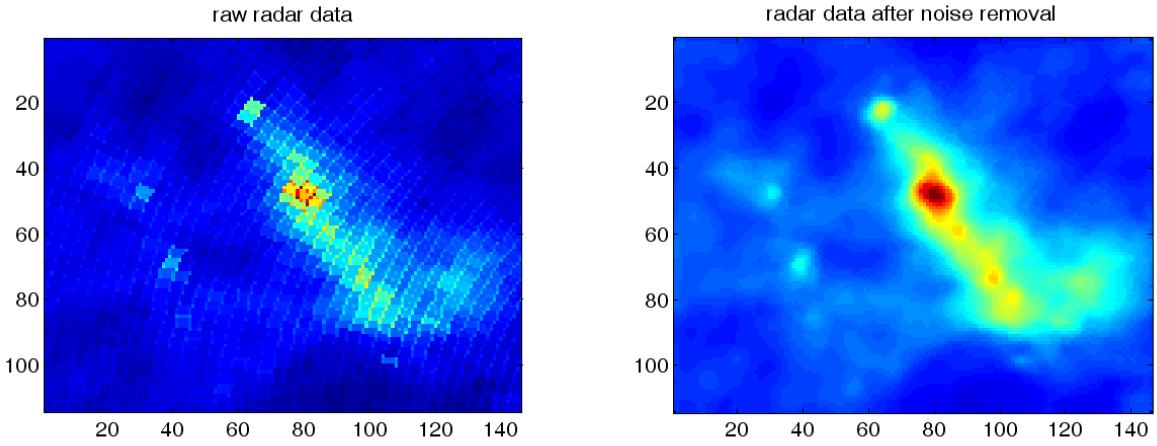

Figure A18. The raw radar image for Oahu (left) and the corresponding one after noise removal (right).

Rainfall Maps Derived from MM5 Mesoscale Meteorological Model

Beginning in 2004, the University of Hawai‘i at Mānoa Meteorology Department's Rain and Wind Study Group has been running the PSU/NCAR MM5 model, a limited-area, non-hydrostatic, terrain-following sigma-coordinate model for weather forecasting and climate studies. MM5 is designed to simulate or predict mesoscale atmospheric circulation (Dudhia, 1993).

At the time of this analysis, MM5 model had been run daily from 01 January 2004 to 31 December 2009. For each day, three model runs were done with three different model domain configurations to produce high-resolution simulations for each individual island as well as the State of Hawai‘i. Run 1 includes four two-way nested levels with horizontal resolutions of 40.5, 13.5, 4.5, and 1.5 km. At nest level four of Run 1, there are two separate nested domains, one covering O‘ahu Island (Figure A19, the other covering Kaua‘i Island (Figure A20); Run 2 covers the Big Island with three nest levels at horizontal resolutions of 81, 27, 9, and 3 km (Figure A21). Run 3 has the same resolution configuration as Run 2 except that the 3-km domain covers Maui (Figure A22). The 9-km domain in Run 3 covers the entire State of Hawai‘i (Figure A23). The model was configured with 28 vertical levels from the surface to the 100-hPa level. The full sigma levels are 1.0, 0.998, 0.994, 0.99, 0.985, 0.98, 0.97, 0.945, 0.91, 0.865, 0.82, 0.79, 0.76, 0.72, 0.68, 0.63, 0.58, 0.52, 0.475, 0.425, 0.375, 0.325, 0.275, 0.225, 0.175, 0.125, 0.075, 0.025, and 0.0.

The physics options for the simulations are the same as those used in Nguyen et al. (2010). Cumulus parameterization, which represents sub-grid scale vertical fluxes and rainfall due to convective clouds producing column moisture, temperature tendencies, and surface convective rainfall, was set using the Grell's cumulus scheme (Grell, 1993), which features quasi-equilibrium in the rate of convective destabilization closure as well as single updraft and downdraft properties. Grell's is a mass-flux type scheme, with compensating subsidence, and is the most suitable option among the cumulus parameterization choices for island-scale resolutions.

The Planetary Boundary Layer (PBL) parameterization, which represents sub-grid vertical fluxes due to turbulence by an unstable boundary layer providing column tendencies for heat, moisture, clouds and momentum, was set using the Medium Range Forecast (MRF) (Hong and Pan, 1996) PBL scheme with nonlocal mixing.

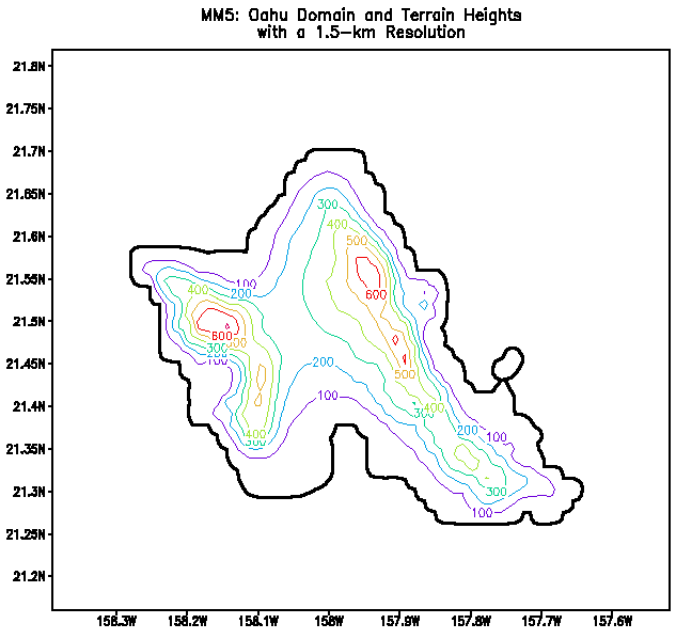

Figure A19. The 1.5-km resolution Oahu domain with terrain height contours. The interval is 100 m.

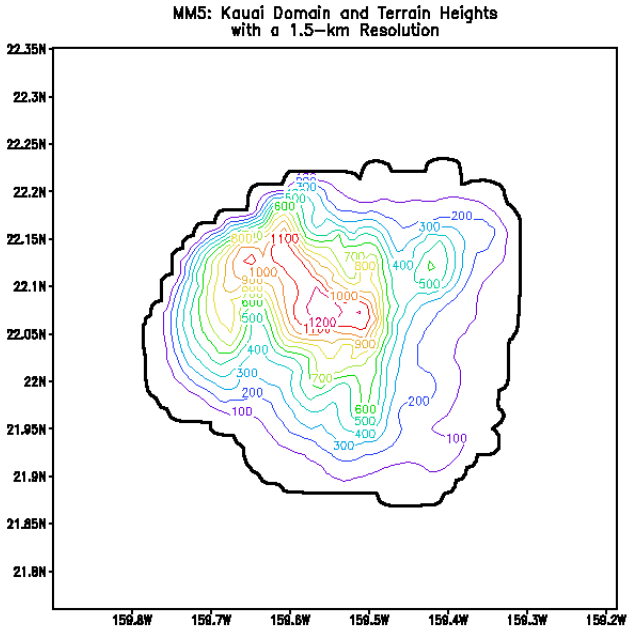

Figure A20. The 1.5-km resolution Kauai domain with terrain height contours. The interval is 100 m.

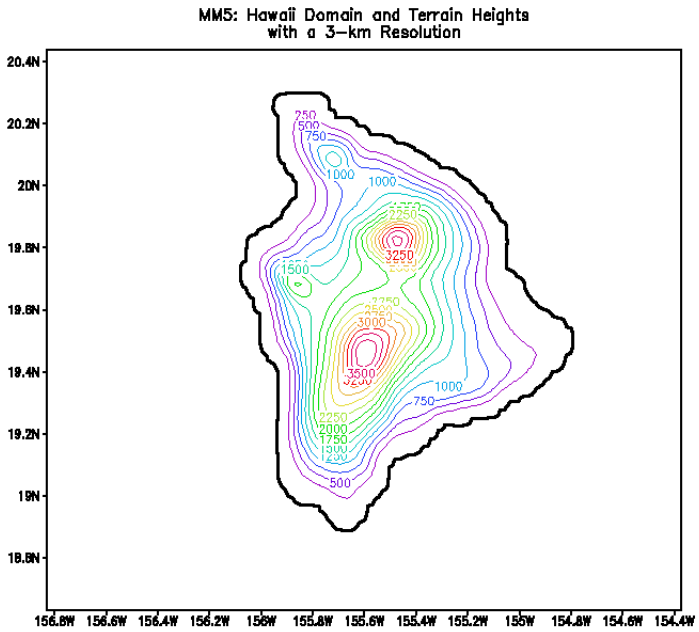

Figure A21. The 3-km resolution Big Island domain with terrain height contours. The interval is 250 m.

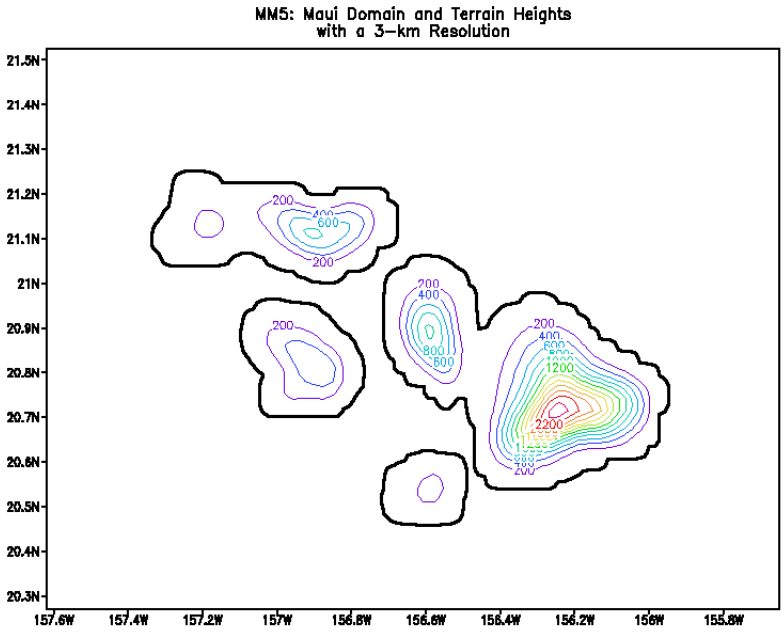

Figure A22. The 3-km resolution Maui domain with terrain height contours. The interval is 200 m.

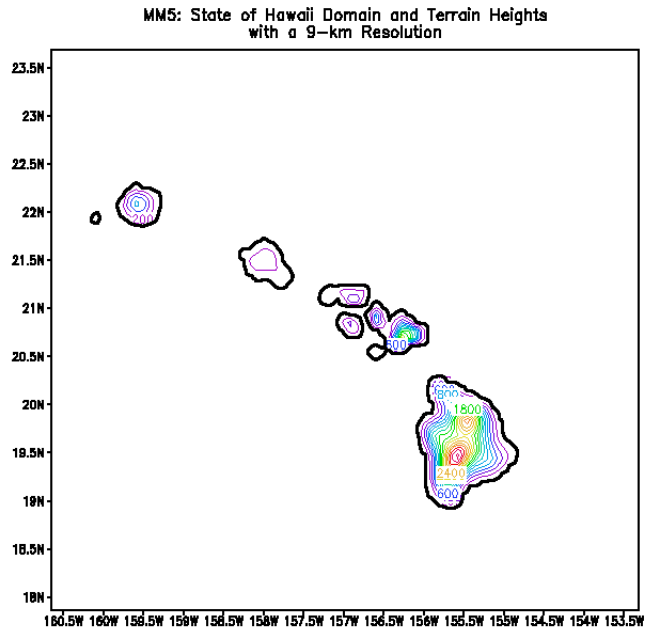

Figure A23. The 9-km resolution State domain with terrain height contours. The interval is 200 m.

Explicit microphysics, which represents the treatment of clouds and precipitation processes on the resolved scale and provides tendencies for temperature, all moist variables, and surface non-convective rainfall as well as information about clouds and radiation, was set using the warm rain microphysics scheme (Hsie et al., 1984). The warm rain scheme does not consider an ice phase.

The radiation parameterization, which represents radiative effects in the atmosphere and on the surface providing downwelling longwave and shortwave fluxes for the surface as well as column temperature tendencies due to vertical radiative flux divergence, was set using the Cloud Radiation scheme (Dudhia, 1989). The Cloud Radiation scheme provides atmospheric radiative effects due to modeled clouds without calling on any other surface radiation scheme.

Surface parameterization, which represents the effects of land and water surfaces and provides information on sensible and latent heat fluxes as well as soil temperature and moisture profiles, was set using the National Centers for Environmental Prediction, Oregon State University, Air Force, Hydrologic Research Lab (NOAH) land surface model (LSM) (Chen and Dudhia, 2001). The vegetation cover and soil properties over Hawai‘i for the Noah LSM were compiled by Zhang et al. (2005a). The Noah LSM predicts soil temperature, soil moisture, canopy water, and snow cover in four layers (10, 30, 60, and 100 cm thick).

Sea surface temperature (SST) is updated with SST observations of 0.5° resolution at the time of initialization from the NCEP SST analysis. The GFS output, with a horizontal resolution of 1°x1°, is used to initialize the daily 36-hour runs. Due to the low resolution of the GFS data, initial conditions from GFS cannot properly represent soil moisture for the state of Hawai‘i. To generate soil moisture data, soil moisture, and soil temperature input for the LSM are spun up for two months prior to the simulation period (Yang et al., 2005) using updated soil moisture and soil temperature. The 24-hour forecasts of the soil moisture and soil temperature of the previous day are used to update the initial conditions for the model for the following day's simulation. The 24-hour model forecast, from the 12th to the 35th hour, is used as the simulated diurnal cycle for each day.

PRISM Rainfall Maps

One of the predictor datasets used to create the final rainfall atlas maps is the PRISM dataset. PRISM (Parameter-elevation Regressions on Independent Slopes Model) is a climate mapping model developed by Christopher Daly at Oregon State University in 1993 (Daly et al., 1994). PRISM assumes that elevation is the most important factor in determining precipitation and has been shown to outperform standard geostatistical methods. The model creates a unique climate-elevation regression function at each cell of the digital elevation model (DEM) and each station is assigned a weight based on spatial variations caused by elevation, vertical layer (inversion in atmosphere), terrain orientation, coastal proximity and topographic position. Digital monthly precipitation maps were created for the entire US (including Hawai‘i), first for the 1961-1990 time period, then updated for the 1971-2000 mean period. PRISM used a total of 442 stations for Hawai‘i (including 20 "estimated" stations), at a resolution of ~450m (Daly et al., 2006). The majority of its data came from the daily NCDC database, with some contributions from smaller networks (e.g., USGS, HaleNet, RAWS). The annual map for Kauai 1971-2000 is shown in Figure A24.

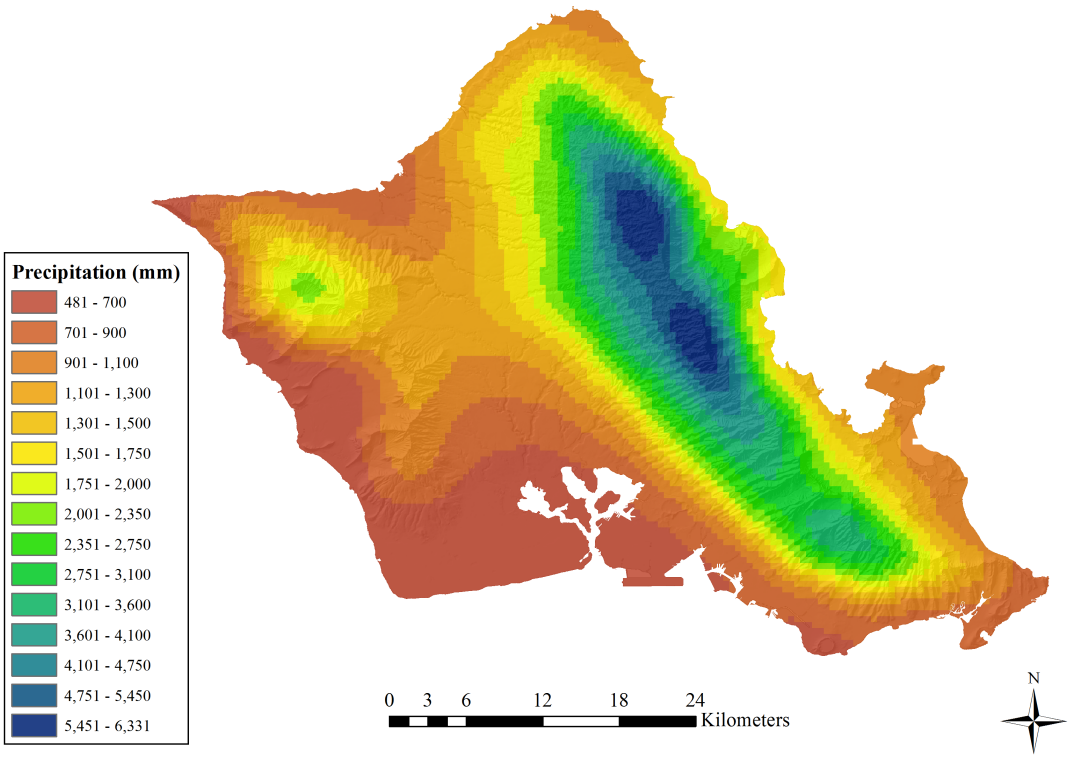

Figure A24. PRISM annual map of O‘ahu, 1971-2000.

Mapping Rainfall by Fusing Different Data Sources

Data Fusion Framework

We mapped rainfall by integrating rainfall gage measurements, vegetation analysis, and predictor data sets, such as radar rainfall, MM5 model simulated rainfall, and PRISM rainfall maps, using a methodology based on Bayesian statistics (Bogaert and Fasbender, 2007). In the framework of this statistical approach, each type of data provides evidences for estimating the true rainfall at a given spatial location, with a certain error associated with it (Figure A25). For the raingage measurements, we assume that there is no bias between the measurements and the true rainfall, but the raingage measurements at each location might have different precision (uncertainty). Predictor datasets (radar, MM5, and PRISM) could have different biases in addition to uncertainty. For some areas where no nearby raingages, we used virtual raingage stations based on vegetation analysis.

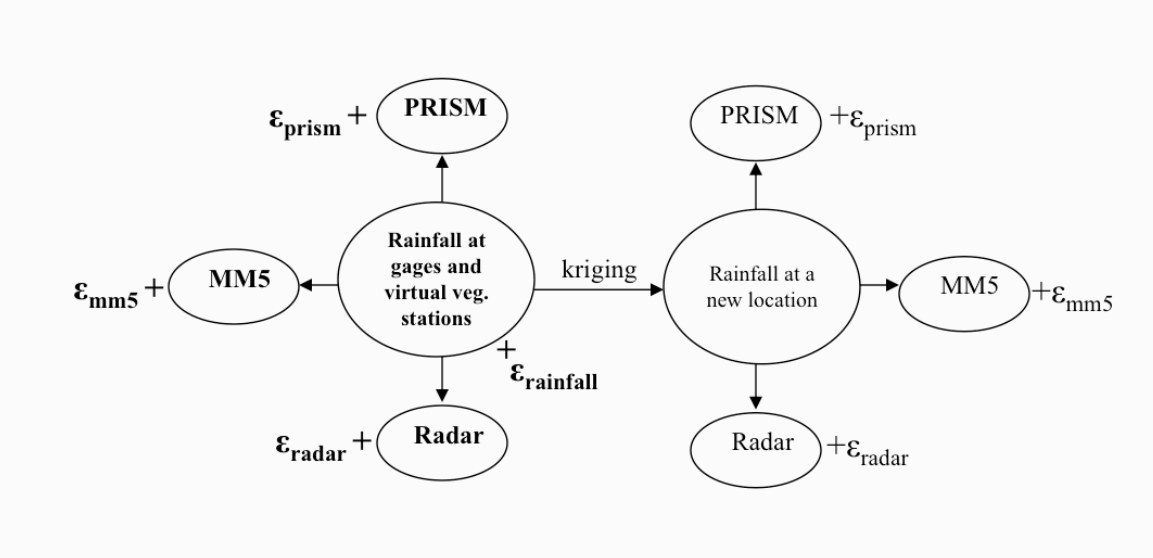

Figure A25. Diagram showing the framework for the Bayesian data fusion as applied in our analysis.

Assume rainfall gage measurements $\mathbf{z} = [z_1,\ldots,z_n]$ are available at spatial locations $\mathbf{x_z} = [x_1,\ldots,x_n]$. At these locations, predictor information $\mathbf{y} = [y_1,\ldots,y_n]'$ is also available I the form of the predictor data sets. The problem is to predict the rainfall z_0 at a new location x_0 where only predictor information y_0 is available, which requires to know the conditional probability $p(z_0 | y_0, \mathbf{z}, \mathbf{y})$. The relationships between z_0, y_0, **z, y** within the Bayesian network are illustrated in Figure A26.

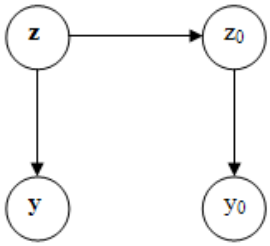

Figure A26. The Bayesian network for rainfall mapping

The conditional dependency (edge) between **z** to z_0 means that **z** and z_0 are spatially correlated. The edges between **z** to **y** or z_0 to y_0 means that the predictor information is dependent on the actual rainfall. For example, the radar measurements are related to rainfall gage measurements. Note that there are no edges between **y** and y_0, which means that **y** and y_0 are independent given **z** and z_0. This is the conditional independent assumption. Based on the Bayesian network in Figure A26, we know that

$$p(z_0 \mid y_0, \mathbf{z}, \mathbf{y}) \propto \frac{p(z_0 \mid \mathbf{z})\, p(z_0 \mid y_0)}{p(z_0)}, \tag{7}$$

This allows us to breathe problem into two parts: 1) the spatial dependence (or autocorrelation) of rainfall $p(z_0 \mid \mathbf{z})$, and 2) the univariate conditional distribution of rainfall at a specific location $p(z_0 \mid y_0)$. The first and second part can be implemented with kriging using gage rainfall and regression with predictor data (radar, PRISM, and MM5), respectively.

Kriging

The rainfall measurements have uncertainties due to gap-filling, location, and small sample. These three types of uncertainties were combined into one error estimate and used in ordinary kriging with measurement errors. Some gages could have relatively large measurement errors based on our calculation, but they might be the only stations within a large area of land due to the relatively sparse gage network. To increase the influence of rainfall gages measurements on the kriging map, we arbitrarily set the variance of a rainfall gage measurements to zero if there are no rainfall gages within a 1,000-m radius surrounding it. Kriging with raingage measurements errors was done using the mGstat Matlab Toolbox (Hansen, 2011). Figure A27 shows an example of ordinary kriging with and without measurement errors.

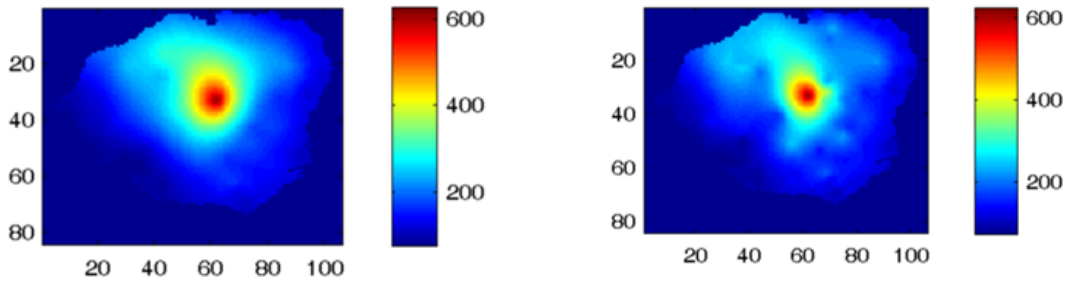

Figure A27. Ordinary Kriging with (left) and without (right) measurement errors.

Regression of Rainfall Based on Predictor Datasets

As shown in Eq. (7), the estimation of rainfall requires knowledge about the distribution of rainfall conditioned on individual predictor datasets (radar, MM5, and PRISM maps). If we assume such distributions are Gaussian, we need to know the conditional mean and variance at a given value of the predictor data. We used a power function model to capture the positive relationship between rainfall and any predictor dataset. An example of the power function model that quantifies the relationship between rainfall and radar imagery for a given month for O‘ahu is shown and the associated conditional mean rainfall map for that month are shown in Figure A28 (top and bottom, respectively).

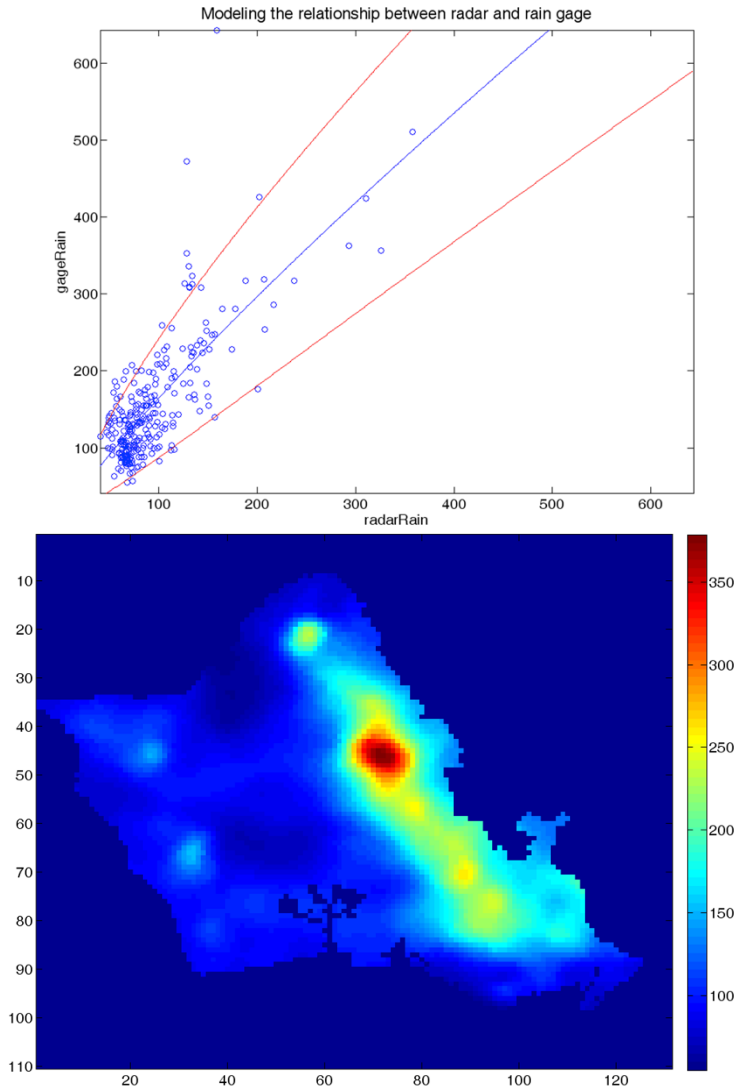

Figure A28. Regression modeling of PRISM and rainfall at a given month (top) and its associated conditional mean rainfall map (bottom).

Besides the conditional mean, the variance conditioned on a given value of the predictor data also has to be estimated. One approach to estimating the conditional variance is to simply use the confidence interval of the regression line. However, such an approach fails to consider that the spatial dependence of errors may not be well predicted. Figure A29 (top) show that this approach produces a variance map that is very similar to the mean map (Figure A28, bottom). Instead, we used a locally-weighted interpolation approach in a 2-dimensional geographic space to estimate variance at any given spatial location (Figure A29, bottom).

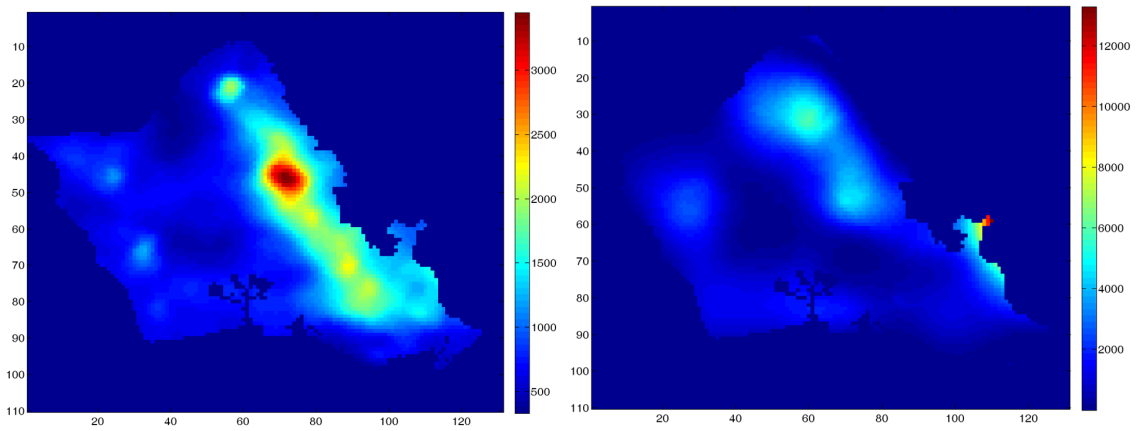

Figure A29. Conditional variance maps based on conditional interval (left) and local weighting (right).

Rainfall Mapping by Fusing All Data

The rainfall estimate based on Bayesian data fusion is essentially an average of kriging and conditional means of individual predictor dataset weighted by their respective spatially-dependent variances (Figure A30). The kriging variance map has very low values at and near the gages, where the fused maps become very localized. To avoid this problem, we smooth the kriging variance map using a Gaussian filter before fusion. Although this can produce a smoother rainfall map in general, it also has the side effect of allowing disagreement between rainfall measurements and maps at the gage. To alleviate this problem, we keep the kriging variance of selected stations, especially those near local rainfall maxima unsmoothed, to prevent them the maximum rainfall values from being reduced.

The spatial distribution of rainfall uncertainty is mapped using the weighted average of the individual predictors' variance. In certain areas of the rainfall uncertainty maps, some artifacts were produced by fusion of very different variance maps from kriging and the predictor datasets (PRISM, MM5, and radar), which were removed by a Gaussian filter.

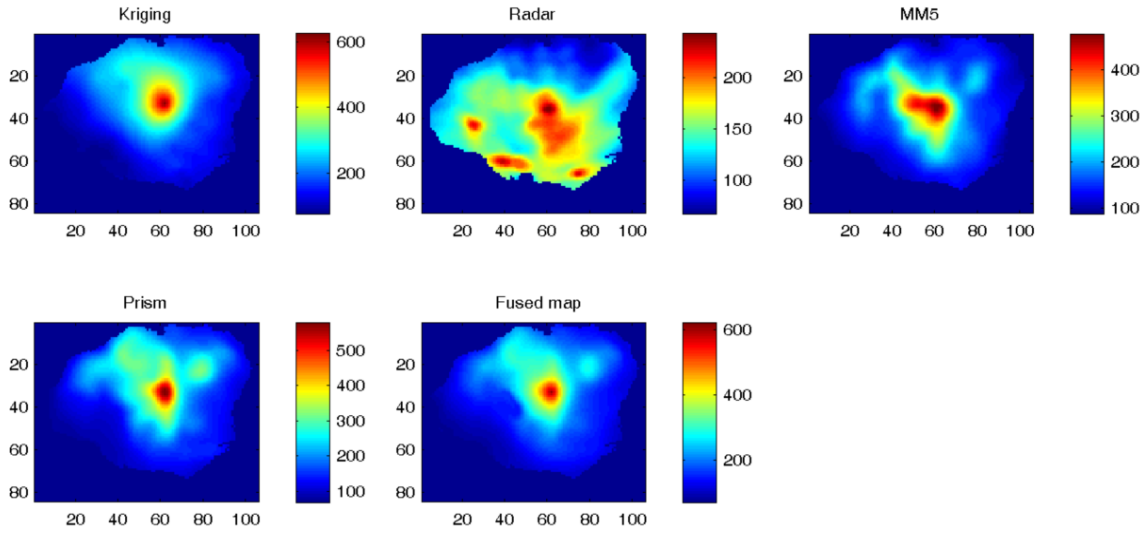

Figure A30. Rainfall mapping by fusing rainfall gages (by kriging), radar, MM5, and PRISM data.

For each island, each month, all predictor datasets were tested. In most cases, however, fused maps using all data were judged to be poor representations of the actual rainfall patterns. Because of high variance and/or spurious patterns resulting from their use, one or more predictor datasets were excluded in the analysis of the final fused rainfall maps for all but 2 of 72 island-months (Table A7). PRISM was the most frequently used predictor (60), followed by MM5 (22) and radar (3).

Table A7. Predictor datasets used to map rainfall for each island-month.

Month	Kaua‘i	O‘ahu	Hawai‘i	Maui	Moloka‘i	Lāna‘i
Jan	P	M	P	P	P	P
Feb	P	M	P	P	P	P M
Mar	P	P R	P	P	P	P M
Apr	P	M	P	P	P	P M
May	P	P M	P	P	P	P M
Jun	P	P M	P	P	P M	P M
Jul	P	P M	P	P	M	P M
Aug	P	M	P	P	M	P
Sep	P	M	P	P	P	P M
Oct	P	P M R	P	P	M	P
Nov	P	P M R	P	P	P	P
Dec	P	P	P	P	P M	P

P=PRISM, M=MM5, and R=Radar.

Appendix References

Bean, C., Juvik, J.O., and Nullet, D. 1994. Mountain evaporation profiles on the island of Hawai‘i. *Journal of Hydrology* 156: 181-192.

Chen, F., and Dudhia, J. 2001: Coupling an advanced land surface-hydrology model with the Penn State-NCAR MM5 modeling system. Part I: Model implementation and sensitivity. *Monthly Weather Review* 129**,** 569–585.

Chu, P.S., and Chen, H. 2005. Interannual and Interdecadal Rainfall Variations in the Hawaiian Islands. *Journal of Climate* 18: 4796-4813.

Cuddihy, L., and Stone, C. P. 1990. Alteration of native Hawaiian vegetation: effects of humans, their activities and introductions. Cooperative National Park Resources Studies Unit, University of Hawai‘i, Mānoa.

Daly, C., Neilson, R.P., and Phillips, D.L. 1994. A statistical-topographic model for mapping climatological precipitation over mountainous terrain. *Journal of Applied Meteorology* 33: 140-158.

Daly, C., Smith, J., Doggett, M., Malbleib, M., and Gibson, W. 2006. *High-Resolution Climate Maps for the Pacific Basin Islands, 1971-2000.* Oregon State University. Pacific West Regional Office: National Park Service.

Doviak, R.J., and Zrnić, D.S. 1984. *Doppler Radar and Weather Observations.* Academic Press, 593 pp.

Dudhia, J., 1989. Numerical study of convection observed during the Winter Monsoon Experiment using a mesoscale two-dimensional model**.** *Journal of the Atmospheric Sciences* 46**:** 3077–3107.

Dudhia, J., 1993: A nonhydrostatic version of the Penn state-NCAR mesoscale model: validation tests and simulation of an Atlantic cyclone and cold front. *Monthly Weather Review* 121: 1493–1513.

Eischeid, J.K., Pasteris, P.A., Diaz, H.F., Plantico, M.S., and Lott, N.J. 2000. Creating a serially complete, national daily time series of temperature and precipitation for the western United States. *Journal of Applied Meteorology* 39: 1580-1591.

ESRI. 2009. ArcGIS Version 9.3. Environmental Systems Research Institute.

Gagne, W.C., and Cuddihy, L.W. 1990. Vegetation. In W. L. Wagner, D. R. Herbst, and S. H. Sohmer (eds.), *Manual of the Flowering Plants of Hawai‘i*. University of Hawai‘i and Bishop Museum Press, Honolulu, pp. 45-114.

Giambelluca, T.W., M.A. Nullet, and T.A. Schroeder. 1986. Rainfall Atlas of Hawai‘i. Technical Report R76, Hawai‘i Department of Land and Natural Resources, Division of Water and Land Development, Honolulu.

Giambelluca, T.W., and Schroeder, T.A. 1998. Climate. In J. O. Juvik, S. P. Juvik, and T. R. Paradise (eds.), *Atlas of Hawai‘i*. University of Hawai‘i Press, Honolulu, pp. 49-59.

Giambelluca, T.W., Diaz, H.F., and Luke, M.S.A. 2008. Secular temperature changes in Hawai‘i. *Geophysical Research Letters* 35, L12702.

Gon, S.M., III, Dorfman, D.S., Matsuwaki, D.H., and EcosystemDataGroup. 1998. Ecosystem GIS Data. GIS Data on CD-ROM. Hawai‘i Natural Heritage Program, Honolulu.

Gon, S. M., III. 2006. The Hawai‘i Gap Analysis Project Final Report. University of Hawai‘i, Research Corporation of the University of Hawai‘i, Honolulu, HI. 163 pages.

Grell, G. A., 1993: Prognostic evaluation of assumptions used by cumulus parameterizations. *Monthly Weather Review* 121: 764–787.

Hansen, T.M. 2011. mGstat: A Geostatistical Matlab toolbox http://mgstat.sourceforge.net. Last accessed on March 1, 2011.

Hillebrand, W. 1888. *Flora of the Hawaiian Islands*, Facsimile reprint of the original edition. Hefner Publishing Co., New York.

Holdridge, L.R. 1967. *Life Zone Ecology*. Tropical Science Center, San Jose, Costa Rica, 206 pp.

Hong, S.-Y., and Pan, H.L. 1996: Nonlocal boundary layer vertical diffusion in a medium-range forecast model. *Monthly Weather Review* 124: 2322–2339.

Horn, J.W., and Kunz, T.H. 2008. Analyzing NEXRAD doppler radar images to assess nightly dispersal patterns and population trends in Brazilian free-tailed bats (*Tadarida brasiliensis*). *Integrative and Comparative Biology* 48: 24-39.

Hsie, E.-Y., Anthes, R.A., and Keyser, D. 1984. Numerical simulation of frontogenesis in a moist atmosphere. *Journal of the Atmospheric Sciences* 41**:** 2581–2594.

Jacobi, J.D. 1989. Vegetation maps of the upland plant communities on the islands of Hawai‘i, Maui, Moloka‘i, and Lāna‘i. Technical Report 68, Cooperative National Park Resources Studies Unit, University of Hawai‘i, Department of Botany, Honolulu.

Jacobi, J.D. 1990. Distribution maps, ecological relationships, and status of native plant communities on the island of Hawai‘i. Ph.D. dissertation. University of Hawai‘i at Mānoa, Honolulu, 290 pp.

Juvik, J.O., Singleton, D.C., and Clarke, G.G. 1978. Climate and water balance on the island of Hawai‘i. In J. Miller (ed.), Mauna Loa Observatory, A 20th Anniversary Report. U.S. Department of Commerce, National Oceanic and Atmospheric Administration, Environmental Research Laboratories.

Juvik, J.O., DeLay, J.K., Kinney, K.M., Hansen, E.W. 2010. A 50th anniversary reassessment of the seminal ‘Lanai fog drip study’ in Hawai‘i. *Hydrologic Processes* 25: 402-410.

Kucera, P.A., Krajewski, W.F., and Young C.B., 2004. Radar beam occultation studies using GIS and DEM technology: an example study of Guam. *Journal of Atmospheric and Oceanic Technology* 21: 995–1006.

LeMone, M., and Pennell, W. 1976. The relationship of trade wind cumulus distribution to subcloud layer fluxes and structure. *Monthly Weather Review* 104: 524–539.

Maddox, R.A., Zhang, J. Gourley, J. J., and Howard, K.W. 2002. Weather radar coverage over the contiguous United States. *Weather Forecasting* 17: 927-934.

Major, J. 1951. A functional, factorial approach to plant ecology. *Ecology* 32: 392-412.

Nguyen, H.V., Chen, Y.-L., and Fujioka F., 2010. Numerical Simulations of island effects on airflow and weather during the summer over the Island of Oahu. *Monthly Weather Review* 138: 2253–2280.

Paulhus, J.L., and Kohler, M.A. 1952. Interpolation of missing precipitation records. *Monthly Weather Review* 80: 129-133.

Price, J., Gon III, S.M., Jacobi, J.D., Matsuwaki, D. 2007. Mapping plant species ranges in the Hawaiian Islands: developing a methodology and associated GIS layers. Hawai‘i Cooperative Studies Unit Technical Report HCSU-008. University of Hawai‘i at Hilo, Hilo, Hawai‘i.

Ripperton, J. C., and E. Y. Hosaka. 1942. Vegetation zones of Hawai‘i. *Hawai‘i Agricultural Experiment Station Bulletin* 89: 1-60.

Rock, J.R. 1913. *The Indigenous Trees of the Hawaiian Islands*. Charles E. Tuttle Co., Rutland, Vermont and Tokyo, Japan.

Sherrod, D.R., Hagstrum, J.T., McGeehin, J.P., Champion, D.E., and Trousdell, F.A. 2006. Distribution, 14C chronology, and paleomagnetism of latest Pleistocene and Holocene lava flows at Haleakala volcano, Island of Maui, Hawai‘i: A revision of lava-flow hazard zones. *Journal of Geophysical Research* 111: B05205.

Stevens, B. 2005. Atmospheric moist convection. *Annual Review of Earth and Planetary Sciences* 33: 605-643.

Thornthwaite, C.W. 1948. An approach towards a rational classification of climate. *Geographical Review* 38: 55-94.

Wang, X.L., Wen, Q.H., and Wu, Y. 2007. Penalized maximal t test for detecting undocumented mean change in climate data series. *Journal of Applied Meteorology and Climatology* 46: 916-931.

Wolfe, E.W., and Morris, J. 1996. Geologic Map of the Island of Hawai‘i (scale 1:100,000). U.S. Geological Survey, Miscellaneous Investigation Series Map I-2524-A.

Yang, Y., Chen, Y.-L., and Fujioka, F.M. 2005. Numerical simulations of the island induced circulations for the island of Hawaii during HaRP. *Monthly Weather Review* 133: 3693–3713.

Zhang, Y., Y.-L. Chen, S.-Y. Hong, H.-M. H. Juang, and K. Kodama, 2005a: Validation of the coupled NCEP mesoscale spectral model and an advanced land surface model over the Hawaiian Islands. Part I: Summer trade wind conditions and a heavy rainfall event. *Weather Forecasting* 20: 847–872.